



**WESTERN REGION TECHNICAL ATTACHMENT
NO. 99-19
SEPTEMBER 14, 1999**

**AN OBSERVATIONAL STUDY OF A CALIFORNIA
BIGHT COASTAL CONVERGENCE ZONE PRODUCED BY FLOW
INTERACTION WITH MAINLAND TOPOGRAPHY:
PRECIPITATION PRODUCER IN SOUTHERN CALIFORNIA**

Ivory J. Small - NWSO San Diego, CA

[Note: All figures and tables appear on the web page only.]
<http://www.wrh.noaa.gov/wrhq/TA99.html>

Introduction

The topic of low-level flow interacting with varying terrain to produce precipitation is not new, but continues to be a forecasting challenge, especially in the West. Some well-known, low-level flow/terrain interactions are the Puget Sound Convergence Zone (Whitney et al. 1993) in northwest Washington State, and the Denver Convergence - Vorticity Zone (Szoke et al. 1984). These are locations where, under certain conditions, mesoscale convergence zones develop. Trade wind interaction with the Hawaiian Islands (Wang and Chen 1998) is another example.

In the Bight Region of southern California (Fig. 1) there is a very significant flow/terrain interaction that results in the production of showers and even thunderstorms over the coastal waters and locally inland over the coastal areas. A convergence zone appears to develop due to a moist, frequently unstable, flow of marine air toward the coast interacting with the rugged southern California terrain as well as interacting with the low-level flow generated by that terrain. There are several ways in which this can occur.

A convergence zone can develop between the comparatively light (mainly nocturnal) boundary layer flow in the coastal areas, (which frequently develops into a land breeze front), and the generally stronger (mainly post-frontal) low-level flow toward the coast. The convergence zone can result in showers and thunderstorms. This type of convergence zone seems to be more prevalent in the late night through mid morning hours. This may be a reflection of the flow "feeling the terrain and terrain-induced boundary layer" more readily during these hours. The boundary generally dissipates when the sea breeze enhances the westerly flow and the nocturnal boundary layer inland dissipates. The nocturnal boundary layer over the coastal areas and associated convergence zone forms even when the synoptic scale pressure gradient is west to east due to high pressure over the Bight, and low pressure inland (this west to east gradient is known locally as an *onshore pressure gradient*, and the low-level flow is known as *onshore flow*).

Hales (1985) speculated that frictional convergence may result from the "unique

juxtapositioning of the coastline and mountains". So frictional convergence may also be due to the onshore low-level flow over the Bight experiencing higher friction as it flows inland, hence convergence and uplift in the vicinity of the coastline. A more detailed discussion can be found in Western Region Technical Attachment No. 87-04.

Another situation under which a convergence zone can develop is when the characteristics of the flow are such that there is blocking of the low-level flow by the coastal mountains of southern California, resulting in a convergence zone. This "blocking" in the southern California Bight has been the topic of research for some time, but mainly for warm season Catalina Eddy cases (Clark and Dembek 1991; Rosenthal 1968; Wakimoto 1987). Although the focus of this Technical Attachment (TA) is convergence zone formation due to flow interaction with mainland topography, it should be mentioned that flow interaction with the islands in the Bight can also produce convergence zones.

It is instructive to consider the Froude number when observing low-level flow/terrain interactions. A good source of information concerning Froude number for the California Bight is Clark and Dembek (1991).

$$Fr = U/Nh$$

where

U = mean wind speed

N = buoyancy frequency (an indicator of static stability)

h = terrain height

Froude numbers of approximately 1 or less can result in blocking by terrain.

As can be seen from the equation, at night when the low-level winds decrease and the airmass becomes more stable near the surface, the Froude number decreases. Lower Froude numbers result in increased blocking by topography. This might explain, in part, why this coastal convergence zone is frequently a night and morning phenomena, especially when there is west to northwest post-frontal flow. It has been found that the afternoon sea breeze can disrupt the blocked flow associated with a Catalina Eddy. This same type of disruption by the sea breeze appears to occur during post-frontal patterns, resulting in the dissipation of the convergence zone that can develop overnight.

Clark and Dembek also stated that airstreams incident upon topography during a Catalina Eddy probably cannot be characterized by a single value of Froude number. For instance, the lowest levels of the incident airstream might have values less than 0.5 because of the small wind speed, whereas higher levels might have values greater than 0.5. [The same condition is likely to be true for the convergence zone created by blocked flow during post-frontal, (as well as some pre-frontal) situations]. They suggested that simulations with high-resolution multi-level models might be needed to fully examine the eddy. That is

beyond the scope of this TA, as it is meant to be mainly a view of the convergence zone from an observational standpoint.

Since the boundary can be a combination of blocking of a moist onshore flow from the Pacific by a cold, nocturnal boundary layer, at times blocking due to a land breeze (mentioned in Small et al. 1998), frictional convergence, or flow blocked by a formidable mountain barrier and its associated flow, simply labeling it as a land breeze front would not fully describe the phenomena, so "California Bight Coastal Convergence Zone" or simply calling the phenomena a "Coastal Convergence" might be a better description. From this point on, for simplicity, it can be referred to by using "CC".

Although the phenomenon is not yet fully understood, for the purposes of this TA a California Bight Coastal Convergence Zone can be defined as the following:

A mesoscale zone that consists of airflow from the Pacific toward the coast, converging with one or more of the following:

1. *A relatively cold nocturnal boundary layer that can evolve into a land breeze front.*
2. *Terrain-forced flow along the mountains (blocking/barrier jet).*
3. *Downslope flow west of the mountains.*

According to Overland and Bond (1993), blocking of onshore flow at low levels is a common occurrence along the West Coast of the United States, and when it occurs along the East Coast it is often referred to as "cold-air damming." Also mentioned was that for typical atmospheric stratifications, an elevation of 100 m is often sufficient to cause blocking of onshore flow at low levels. With terrain rising abruptly to over 3000 meters in southern California, the onshore flow can easily be blocked. From Doyle and Warner (1993) coastal fronts are shallow (typically less than 500 meters deep) mesoscale boundaries that separate warm, moist oceanic air from cold, dry continental air. They also stated that mechanisms for the initiation of coastal frontogenesis include differential friction, differential diabatic heating, orographical blocking of the upstream flow, and land-sea circulations. It seems that at times the CC displays the characteristics of the coastal front, found on the east coast. This is especially true overnight when a nocturnal boundary layer develops over the mainland areas near the coast.

Before the introduction of Doppler radar and high resolution satellite data, it was very difficult to observe these phenomena with much detail. With the installation of NEXRAD (Next Generation Weather Radar) in the Bight region, along with improved satellite data, these phenomena can now be easily observed.

In addition to the terrain-forced boundaries, there are also boundaries associated with mesoscale cellular convection. Sometimes the two can interact to enhance the convection. This will be seen later in this TA.

In order to examine these phenomena, some background theory concerning convection over the ocean will be presented. Several well-known examples from various locations will be highlighted to use as comparisons to cases in southern California. Case studies in southern California will also be presented. There is a brief discussion of some of the more important points in the TA with some final thoughts on the importance of understanding these phenomena.

Brief Overview of Convection over the Ocean

In mid-latitudes, convection over the ocean, or other very large bodies of water, is most frequently observed in the winter season when cold polar air behind a mid-latitude frontal system moves over a relatively warm ocean. The warming influence of the ocean surface is a principal mechanism for destabilizing the polar airmass by warming the lowest levels and adding moisture to the airmass. Horizontal roll convection (cloud streets) and mesoscale cellular convection (polygonal-shaped open and closed cells) can develop. The detailed theory behind the formation of roll-type and mesoscale cellular convection can be further obtained from Agee et al. (1973). Examples of these phenomena will be seen throughout this TA.

Some Examples of Convection over Large Bodies of Water

A. Lake Effect Convection over the Great Lakes on 7 November 1978

Wintertime cold-air outbreaks over the Great Lakes has been studied both observationally as well as numerically (e.g., Agee and Gilbert 1989; Agee and Hart 1990). With weak boundary layer flow, a convective band tends to form over the lake. Figures 2 and 3 for 7 November 1978 show light land breezes converging over the lake, forming a band.

B. Convection over the Baltic Sea on 11 January 1987

Andersson and Gustafsson (1994) studied convective snowbands over the Baltic Sea (Fig. 4) during a case of cold easterly flow. The satellite picture showed what was called a "gulf band", a "bay band", and a "corner band". The gulf band stretches from the Gulf of Finland, westward over the northern Baltic Sea toward Sweden. It was determined that originally there were other wind-parallel bands stretching westward from the gulf. Eventually, one dominant band formed. They hypothesized that the band formed as either a shore-parallel band resulting from a land breeze circulation along one of the shores, or a mid-lake band generated by land breeze circulations from both shores of the Gulf of Finland (similar to the 7 November 1978 Great Lakes mid-lake band). Also found were the horizontal differences in surface roughness resulted in "coastal convergence", and was important for the formation of the corner band. The bay band was considered to be a result of convergence due to land breeze circulations.

The location and orientation of the CC in southern California appear to depend on the relative strength of the post-frontal onshore flow. This can also be seen with the sea-breeze case in Fig. 5. In the figure there is a synoptic scale low-level gradient flow (westerly) superimposed on the sea breeze circulation. As a result the west coast sea breeze front is moved inland on the west coast of Florida, but the east coast sea breeze front has remained fairly close to the east coast. This adjustment of the location of the band in relation to the coastline seems to be the case in southern California based on the case studies in this TA.

Case Studies of Events in Southern California

CASE A. Catalina Eddy Event on 5-6 November 1998

On 5-6 November 1998, a Catalina Eddy developed in the southern California Bight region. The Catalina Eddy is a shallow cyclonic circulation of approximately 100-200 km that occasionally develops in the California Bight. It mainly occurs below the marine inversion. The circulation develops when the northwesterly flow blocked by the mountains east of San Diego (SAN) are turned north along the coast, then west to complete the circulation. These events have been extensively studied, and detailed information concerning these events can be found in Rosenthal (1968), Wakimoto (1987), Mass and Albright (1989) as well as in Clark and Dembek (1990). Figure 6 shows the 32 km ETA at 1800 UTC 5 November 1998. A circulation center can be seen just southeast of San Clemente Island. This is supported by the surface observation for 1500 UTC 5 November 1998 and 1500 UTC 6 November 1998 in Figs. 7 and 8. The marine layer can be seen in the 1200 UTC 5 November 1998 (Fig. 9) and 0000 UTC 6 November 1998 (Fig. 10) radiosondes from Miramar (NKX). Although the winds were not available on the soundings, the 2048 UTC 5 November 1998 KNKX VAD wind profile (Fig. 11) clearly shows the southerly low-level flow. Finally, satellite imagery in Figs. 12 through Fig. 16 show the progression of the eddy from the mature stage through its dissipation. The key features to notice that there are two boundaries. There are clouds along the boundary that separates the southerly flow over the coastal areas from the slower moving air near the island, and the clouds along the boundary that separate this slower moving air near the islands, and the faster moving northwesterly flow further offshore. [It is interesting to note that in Szoke et al. (1984a) it was stated, concerning the Denver Convergence-Vorticity Zone, that "the exact location and structure of the zone can vary; a single convergence/shear zone is more common than the double boundary structure that occurred on 26 July 1985"]. These two boundaries associated with the Catalina Eddy can be seen on the 1615 UTC 5 November 1998 satellite imagery in Fig. 12. The boundary closest to the coast dissipates by 2345 UTC 5 November 1998 due to the development of a sea breeze, disrupting the southerly flow temporarily (Fig. 13). Notice the boundaries are apparent the following morning at 1615 UTC 6 November 1998, nearly 24 hours later (Fig. 14). It is key to note that the boundary nearest to the coast has redeveloped, whereas the other boundary to the west has persisted from the previous day. As the eddy dissipates the northwesterly flow can shift

closer toward the coast (Figs. 15 and 16). A very similar situation with a boundary near the coast, with another boundary further west can be seen in another Catalina Eddy case on 1800 UTC 20 May 1998 in (Fig. 17) from Martin (1998). These convergent areas associated with eddy events are generally benign, but can produce measurable light rain on occasion (especially when there is rapidly increasing onshore flow, a rapidly deepening marine layer, and a strong inversion). A major difference between the boundaries generated by Catalina eddies and boundaries that produce thunderstorms is the depth of the conditionally unstable layer. Other cases later in this TA will illustrate this point.

CASE B. Coastal Convergence on 14 January 1998

The 1715 UTC 14 January 1998 visible picture (Fig. 18) shows a CC over the California Bight, extending south along the Baja peninsula. Most surface winds over the mainland coastal areas had a weak easterly component, and the flow was likely to be that of a land breeze, seen on the 1200 UTC 14 Jan 1998 NKX raob (Fig. 19). Also notice the nocturnal boundary layer. The airmass was almost saturated up to 4000 feet, then there is no data above 6000 feet. Because the airmass dries out considerably above 4000 feet, the boundary was relatively benign.

CASE C. Coastal Convergence on 26 March 1998

The 0000 UTC 26 March 1998 NKX raob (Fig. 20) showed a post-frontal airmass, which was nearly saturated up to about 8000 feet. This set-up resulted in a CC developing overnight, as indicated on the 1515 UTC 26 March 1998 visible satellite imagery (Fig. 21). The convergence line lies in a northwest to southeast orientation, beginning on the coastline in the north near SNA. It appears that gusty west to northwest winds in the SAN area pushed the CC inland on the southern end. This adjustment of the southern end of the CC is similar to the inland adjustment of the boundary in the Florida case cited earlier.

CASE D. Coastal Convergence on 9 February 1998

The 1200 UTC 9 February 1998 NKX raob showed a post-frontal airmass, which was nearly saturated up to 6000 feet and conditionally unstable (Fig. 22). The flow was unidirectional, and increased steadily with height. The 1200 UTC 9 February 1998 visible satellite imagery showed a CC (Fig. 23). Since the band begins very close to Santa Catalina Island, it is possible that the band may have experienced some additional enhancement due to flow interacting with the island.

CASE E. Coastal Convergence on 5 February 1998

5 February 1998 is a good example of the CC remaining offshore, seen on the 1745 UTC 5 February 1998 visible satellite imagery (Fig. 24). The frontal passage and a wind shift to westerly at CRQ occurred at about 0100 UTC 4 February 1998, about 36 hours earlier, so the post-frontal winds had weakened. There was a line of thunderstorms over the

coastal waters, evident on the 1745 UTC 5 February 1998 visible satellite imagery, and was supported via pilot report at 1747 UTC 5 February 1998. The line can be seen extending to well south of the Mexican Border over the coastal waters. There was a 2-3 mb onshore synoptic-scale pressure gradient from the coast to the deserts, with higher pressure at the coast and lower pressure over the deserts. However, there was calm to light northeasterly flow in the boundary layer over the land areas near the coastline, so the line of thunderstorms remained offshore.

CASE F. Coastal Convergence on 6-8 April 1998

Wang and Chen (1998) examined the interaction between the Trade-Wind Rain bands and the flow on the windward side of the Island of Hawaii. There is a persistent easterly trade wind past Hawaii most of the year, with an August maximum. At night, an offshore land breeze develops on the island, and extends some 10 to 20 km offshore. At the same time, there are rain bands in the trade wind flow moving toward the island-induced land breeze convergence zone. When the rainbands reach the convergence zone between the offshore winds and the trade winds, the echoes in the rain band are enhanced. A southern California example of this type of event appears to be evident in the following 6-8 April 1998 event.

On 6-8 April 1998 a large trough of low pressure was over much of the western states. The trough was nearly stationary, and several weak disturbances moved through the trough, keeping the airmass over southern California moist and unstable. The surface pressure pattern indicated a significant onshore pressure gradient from the coast to the interior (not shown). The 1200 UTC 6 April 1998 raob (Fig. 25) indicated a conditionally unstable airmass below about 6000 feet. The winds were unidirectional and increased steadily with height. The raob was an indication that 6 April 1998 could become a very active day for mesoscale convection. The 1800 UTC 6 April 1998 visible satellite imagery showed extensive open cell convection (Fig. 26). Also bands of convection had developed downwind of San Clemente and Santa Catalina islands. A reverse clearing pattern [when the lower clouds clear over the coastal waters and coastal areas by mid afternoon and over the inland areas later in the day (as opposed to the usual diurnal pattern where the inland areas clear first)] had developed (Fig. 27). This also points toward a deep moist airmass at the lower levels.

The 1200 UTC 7 April 1998 NKX raob (Fig. 28) again showed a conditionally unstable airmass with unidirectional winds steadily increasing with height. The stronger winds over the offshore waters were evident on the 1700 UTC 7 April 1998 surface map (Fig. 29) with 20 knots or more over the coastal waters from the coastal buoy observation in the north southward to San Nicolas Island. The 1500 UTC 7 April 1998 visible satellite imagery (Fig. 30) showed a rather impressive CC that crosses the coastline just east of Santa Catalina Island near SNA, and very active open cell convection in the Bight mainly west of the CC. The 1456 UTC 7 April 1998 KNKX composite reflectivity also shows a band of thunderstorms associated with open cell convection approaching the CC in Fig. 31. By

1543 UTC 7 April 1998 ,the line of thunderstorms interact with the CC and convection is enhanced at the intersection point just south of SNA in Fig. 32. The storm then moves inland and strengthens as shown on the 1743 UTC 7 April 1998 KNKX composite reflectivity in Fig. 33. The 2000 UTC 7 April 1998 visible satellite imagery showed that the CC had dissipated (Fig. 34). A few bands develop downwind of the islands due to interaction of the flow with the islands. Again, a reverse clearing pattern was noted, so the deep moist air mass at the lower levels was still in place.

By the following morning, with the deep moist airmass still in place, the 1430 UTC 8 April 1998 visible satellite imagery showed a well-developed CC over the coastal waters, extending southward along the coast to well south of the Mexican Border (Fig. 35). There were numerous cloud streets over the coastal waters. The cloud streets to the west of the CC were oriented NW-SE, but the southeastern end of the streets bend to the left and intersect the CC with a nearly perpendicular intersection. This was especially true off the coast near the California/Mexican border. This nearly perpendicular intersection was noted in Atkins et al. (1995) for sea breeze fronts (Fig. 36). It appears that the nearly perpendicular intersection is also a feature associated with the CC, and possible with land breeze fronts in other areas.

CASE G. Coastal Convergence on 3-6 December 1997

This case showed what appeared to be two bands of convection over the coastal waters ahead of an approaching cold front. The boundaries can be seen on the 1715 UTC 3 December 1997 1 km visible satellite imagery in Fig. 37 and the 1700 UTC 3 December 4 km visible satellite imagery in Fig. 38. This prompted the author to make a coordination call to the Lead Forecaster (Gomberg) at the Los Angeles/Oxnard National Weather Service Forecast Office during the development of the boundaries to discuss the implications of the boundaries. There were two mechanisms that could result in these boundaries. The first possibility was the easterly component of the low-level flow resulting in weak downslope wind undercutting a moist pre-frontal southerly flow. The second was convergence caused by the moist south to southeast flow being blocked by the coastal mountains. (It is very difficult to determine the contribution of these mechanisms to the development of the boundaries, but nevertheless, by afternoon an explosive convergence zone developed over the coastal waters). At 1715 UTC 3 December, there was low level east to northeast flow to the band nearest to the coastline (the inner CC boundary). Well-defined arcs of clouds marked the inner CC boundary which can be seen on Fig. 37 extending down the coast to near San Clemente Island (NSI). These arcs are possibly the result of northeast flow locally enhanced by the terrain, similar to the accelerations which occur during Santa Ana winds below the "favored" passes and canyons (Small, 1995). The flow can also be seen in the surface data, with northeast flow into the arcs, and southerly flow west of the arcs at 1700 UTC 3 December 1997 (Fig. 39). Even the 1200 UTC 3 December 1997 NKX raob showed weak easterly flow over the coastal waters (Fig. 40). The 1200 UTC 3 December 1997 VBG raob showed stronger southeast flow in Fig. 41.

It had become obvious that a very complex situation had developed over the coastal waters. Still further west an outer CC boundary was in the development stage. The clouds from the inner CC boundary can be seen in Fig. 37 stretching from near Vandenberg (where it resulted in light rain), developing into a series of arcs south along the coast to Santa Catalina Island, then becoming broken up, but continuing to parallel the coast just west of the Baja peninsula. The CC boundary, seen on Fig. 37 and Fig. 38, seemed to stretch from just west of Vandenberg (VBG) southeast to where it intersects the inner CC boundary and continuing down the coast, forming what appears to be one boundary. By 2300 UTC 3 December 1997 the outer CC boundary had moved closer to the coast to the location where the inner CC boundary had been, and strengthened. This can be seen in the 2300 UTC 3 December 1997 1 km visible satellite imagery in Fig. 42 as well as in the 2300 UTC 3 December 1997 4 km visible satellite imagery in Fig. 43.

The following day, about 24 hours later, the 2315 UTC 4 December 1997 1 km visible satellite imagery in Fig. 44 and the 2300 UTC 4 December 1997 4 km visible satellite imagery in Fig. 45 showed the broad CC had moved a bit further east, and even began strengthening on the southern end, off the coast of the Baja peninsula. The quasi-stationary character of the CC during a 24-hour period, even as the entire system was moving east, was consistent with the idea of "blocked flow." The 2315 UTC 4 December 1997 visible satellite imagery from Fig. 44 and Fig. 45 seem to show the shape of the CC conforming to the shape of the coastline from the northern areas to well south of the California border along the Baja Peninsula. Braun et al. (1997) noted that during the Coastal Observations and Simulations with Topography (COAST) experiment, it was found that the cold front in their Fig. 4 also "felt" the terrain, and mirrored the shape of the coastline to some degree.

In addition, the 1200 UTC 4 December 1997 NKX (Fig. 46) and the 1200 UTC 4 December 1997 VBG (Fig. 47) showed what appeared to be a 15 knot jet at about 950 mb on the NKX raob and a 40 knot jet at about 900 mb on the VBG raob. This low-level jet also appears on the raob in Overland and Bond (1993) in their figure 3, which suggests a barrier jet associated with damming phenomena. On 6 December 1997, three days after the initial development of the convergence boundaries in the southern California Bight, a rainfall event with a 30,000+ year return period occurred, possibly as a result of the CC.

Discussion and Conclusion

From the examples it can be seen that CC boundaries form in post-frontal environments under conditions very similar to those found during mesoscale cellular convection. Sometimes a CC will form and split around, or experience enhancement due to the islands. At other times two boundaries can develop in one portion of the CC, and combine to form one boundary in another portion of the CC, resulting in a "Y" shaped feature. Also two boundaries can develop without appearing to be combined on either end, further complicating the problem.

A thorough knowledge of the situations that result in CC activity is very important. This is because frequently when the main area of upward forcing exits the region and downward motions develop over the region, the CC can still activate and produce additional showers and thunderstorms even when areas away from the CC are clear.

Bands that develop near the coast tend to dissipate when the sea breeze develops. However, for the 3-6 December case the boundary did not dissipate. (The case was prefrontal with very strong flow ahead of the system, and the CC was well offshore).

Boating and aviation operations can be adversely affected by CC phenomena. The weather produced by these phenomena can also result in hazardous driving conditions as visibilities can drop rapidly in showers and thunderstorms. These boundaries can be prolific small hail producers when freezing levels fall below about 6000 feet. A more detailed discussion of the exact cause of this phenomenon will follow up this observational approach after further investigation in future research .

Acknowledgments

I would like to thank Armando Garza and Ed Clark for their review, comments, and invaluable suggestions for this TA. I also wish to thank Greg Martin for graphical assistance.

References

- Agee, E. M., Chen, T. S. and K. E. Dowell, 1973: A Review of Mesoscale Cellular Convection., *Bull. Amer. Meteor. Soc.*, **54**: 1004-1012.
- Agee, E. M. and M. L. Hart, 1990: Boundary Layer and Mesoscale Structure over Lake Michigan During a Wintertime Cold Air Outbreak. *J. Atmos. Sci.*, **47**: 2293-2316.
- Agee, E. M. and S. R. Gilbert, 1989: An Aircraft Investigation of Mesoscale Convection over Lake Michigan during the 10 January 1984 Cold Air Outbreak. *J. Atmos. Sci.*, **46**: 1877-1897.
- Andersson, T., and N. Gustafsson, 1994: Coast of Departure and Coast of Arrival: Two Important Concepts for the Formation and Structure of Convective Snowbands over Seas and Lakes. *Mon. Wea. Rev.*, **122**, 1036-1049.
- Atkins, N. T. , R. M. Wakimoto, and T. M. Weckwerth., 1995: Observations of the Sea Breeze Front during CaPE. Part II: Dual-Doppler and Aircraft Analysis. *Mon. Wea. Rev.*, **123**, 944-969
- Bader, M..J. Bader, G. S. Forbes, J. R. Grant, R. B. E. Lilley, and A. J. Waters., 1995: *Images in Weather Forecasting*. Cambridge University Press, New York 499 pp.

Braun, S. A., R. A. Houze Jr. and B. F. Smull, 1997: Airborne Dual-Doppler Observations of an Intense Frontal System Approaching the Pacific Northwest Coast. *Mon. Wea. Rev.*, **125**, 3131-3156.

Clark, J. H. and S. R. Dembek, 1990: The Catalina Eddy Event of July 1987: A Coastally Trapped Mesoscale Response to Synoptic Forcing. *Mon. Wea. Rev.*, **119**, 1714-1735.

Doswell, C. A., 1985: The Operational Meteorology of Convective Weather, Volume II: Storm Scale Analysis. NOAA Technical Memorandum ERL ESG-15. Environmental Sciences Group, Boulder, Colorado. 240 pp.

Doyle, J. D. and Thomas T. Warner., 1993: A Numerical Investigation of Coastal Frontogenesis and Mesoscale Cyclogenesis during GALE IOP 2. *Mon. Wea. Rev.*, **121**, 1048-1077

Hales, J. E., Jr., 1985: Synoptic features associated with Los Angeles Tornado Occurrences. *Bull. Amer. Meteor. Soc.*, **66**, 657-662.

Hubert, L. F., 1966: Mesoscale Cellular Convection. Meteorological Satellite Laboratory Report No. 37, Washington D. C. , 68 pp.

Krueger, A. F., and S. Fritz, 1961: Cellular Cloud Patterns Revealed by TIROS I, *Tellus*, **13**, 1-7

Laird, N. R., D. A. R. Kristovich, R. M. Rauber, H. T. Ochs III, and L. J. Miller, 1995: The Cape Canaveral Sea and River Breezes: Kinematic Structure and Convective Initiation. *Mon. Wea. Rev.*, **123**, 2942-2956.

Martin, G., 1998. Applications of the ETA-10 and ACARS Data to Monitoring and Forecasting Marine Layer Stratus in Southern California. Pending Publication.

Mass, C. F., and M. D. Albright, 1989: Origin of the Catalina Eddy. *Mon. Wea. Rev.*, **117**, 2406-2436.

Mass, C. F., and M. D. Albright, 1987: Coastal southerlies and alongshore surges of the west coast of North America; Evidence of mesoscale topographically trapped response to synoptic forcing. *Mon. Wea. Rev.*, **115**.

Overland, J. E., and N. Bond., 1993: The Influence of Coastal Orography: The Yakutat Storm. *Mon. Wea. Rev.* **121**, 1388-1397.

Riehl, H., 1954: *Tropical Meteorology*. McGraw Hill Book Company, Inc. New York 392 pp.

Rosenthal, J., 1968: A Catalina Eddy. *Mon Wea Rev.*, **96**, 742-743

Small, I., 1995: Santa Ana Winds and the Fire Outbreak of Fall 1993. NOAA Technical Memorandum NWS WR-230. National Weather Service Western Region, P. O. Box 11188, Salt Lake City, UT 84147.

Small, I. J., D. V. Atkin, and T. E. Evans III, 1998: Severe Hail Detection Using VIL Density and Its Application In The Western States. Western Region Technical Attachment No. 98-37, 8pp. National Weather Service Western Region, P. O. Box 11188, Salt Lake City, UT 84147.

Staudenmaier, M., 1995: Convective Horizontal Roll Vortices As Viewed By WSR-88D. Western Region Technical Attachment No. 95-16, 4pp. National Weather Service Western Region, P. O. Box 11188, Salt Lake City, UT 84147.

Szoke, E. J., and R. H. Brady, 1989: Forecasting Implications of the 26 July 1985 Northeast Colorado Tornadoic Thunderstorms Case. *Mon. Wea. Rev.*, **117**, 1834-1860

Szoke, E. J., M. L. Weisman, J. M. Brown, F. Caracena, and T. W. Schlatter, 1984: A subsynoptic analysis of the Denver tornadoes of 3 June 1981. *Mon. Wea. Rev.*, **112**, 790-808

Wang, J. -J., and Y. -L. Chen, 1998: A Case Study of Trade-Wind Rainbands and Their Interaction with the Island-Induced Airflow. *Mon. Wea. Rev.*, **126**, 409-423

Whitney, W. M., R. L. Doherty, B. R. Colman, 1993: A Methodology for Predicting the Puget Sound Convergence Zone and Its Associated Weather. *Wea. Forecasting*, **8**, 214-222.

Secondary Circulations As the Result of Frictional Convergence Along A Coastline. Western Region Technical Attachment No. 87-04, 4pp. National Weather Service Western Region, P. O. Box 11188, Salt Lake City, UT 84147.

Velarde, M. G., and C. Normand, 1980: Convection. *Sci. Amer.*, **243**, 92-109.

Wakimoto, R. M., 1987: The Catalina Eddy and its Effect on Pollution Over Southern California. *Mon. Wea. Rev.*, **115**, 837-855.

**AN OBSERVATIONAL STUDY OF A
CALIFORNIA BIGHT COASTAL CONVERGENCE ZONE
PRODUCED BY FLOW INTERACTION WITH MAINLAND
TOPOGRAPHY:
PRECIPITATION PRODUCER IN
SOUTHERN CALIFORNIA**

**Ivory J. Small
NWSO San Diego, CA
(Figures)**

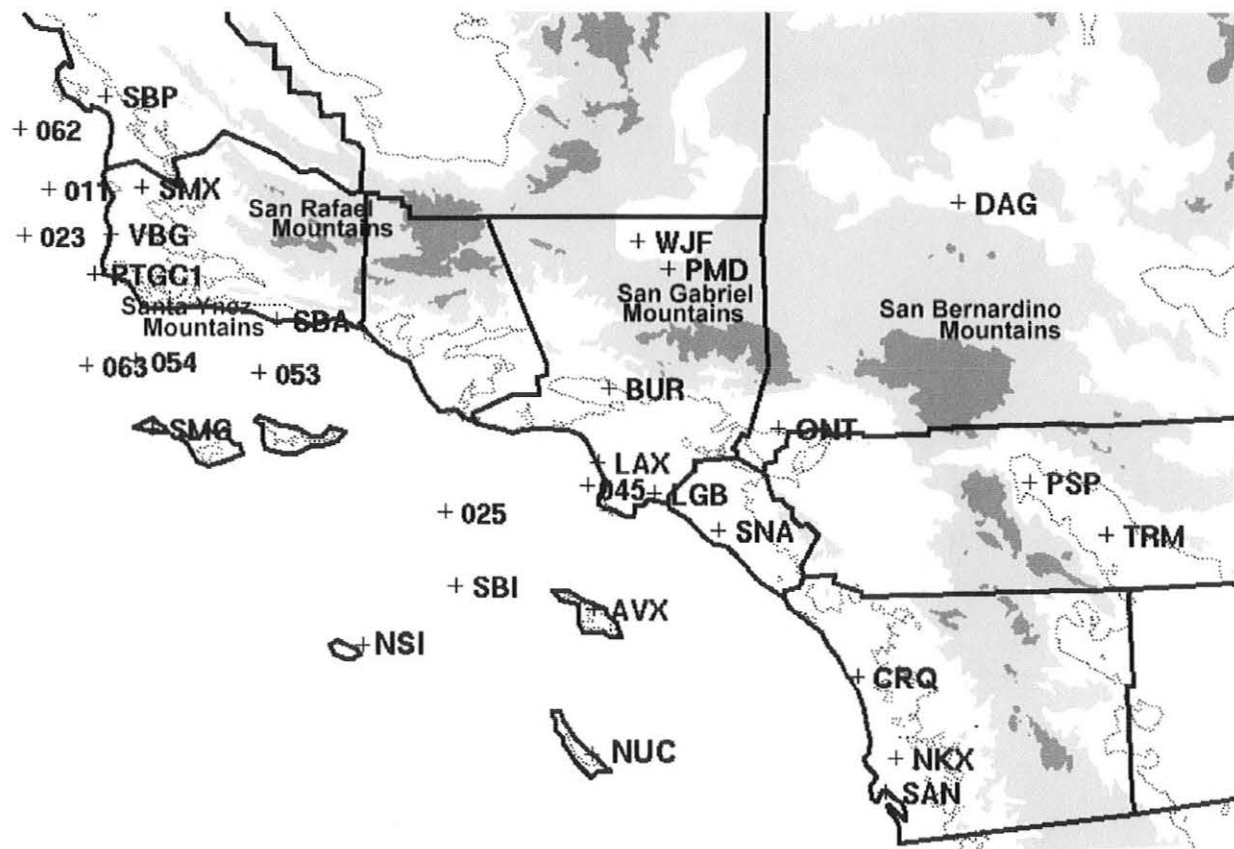


Fig. 1. Topographical features and geographical features in the Southern California Bight Region.

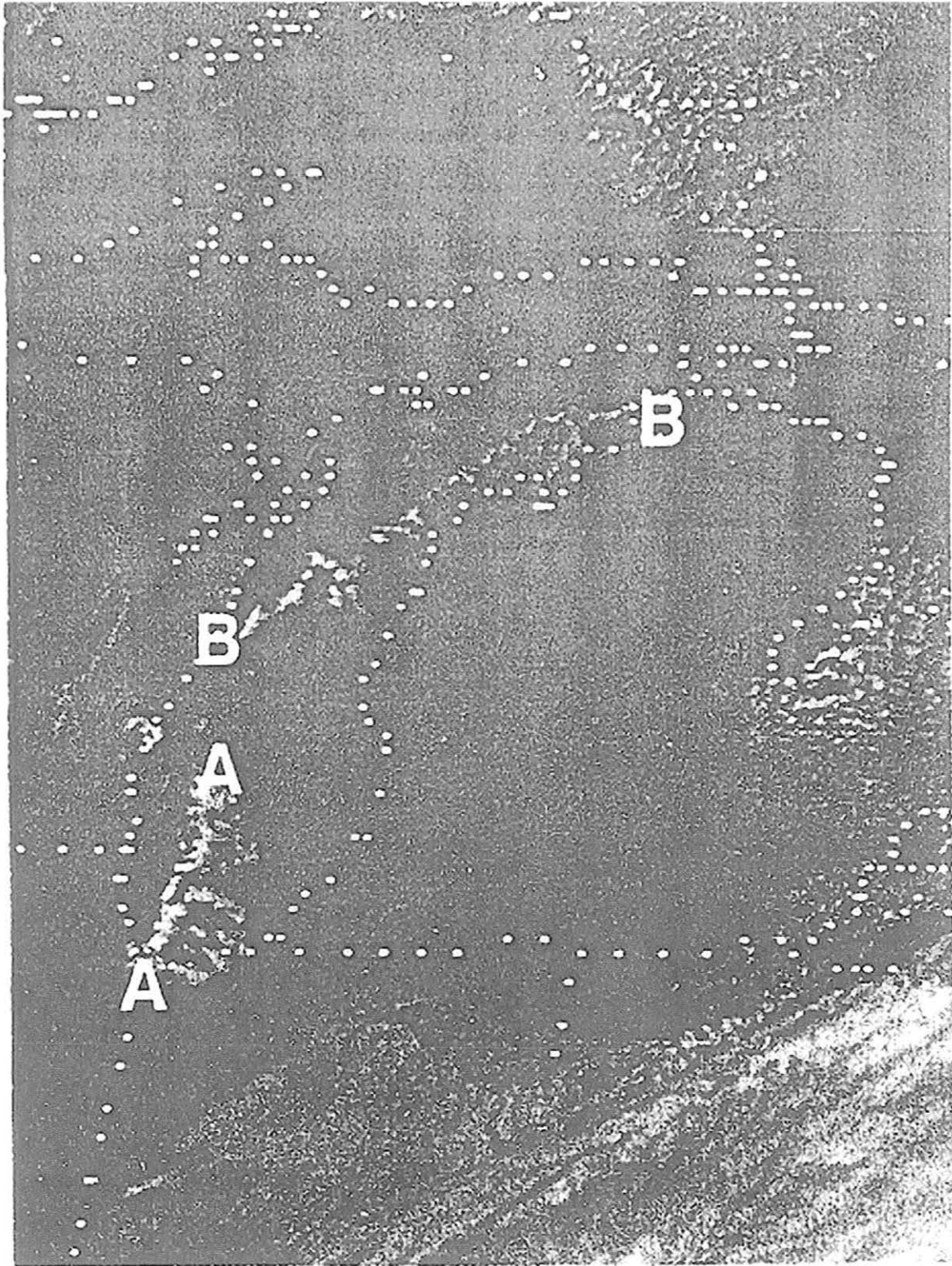


Fig. 2. GOES visible image at 1630 UTC 7 November 1978 showing lake convergence bands (After Bader et al. 1995).

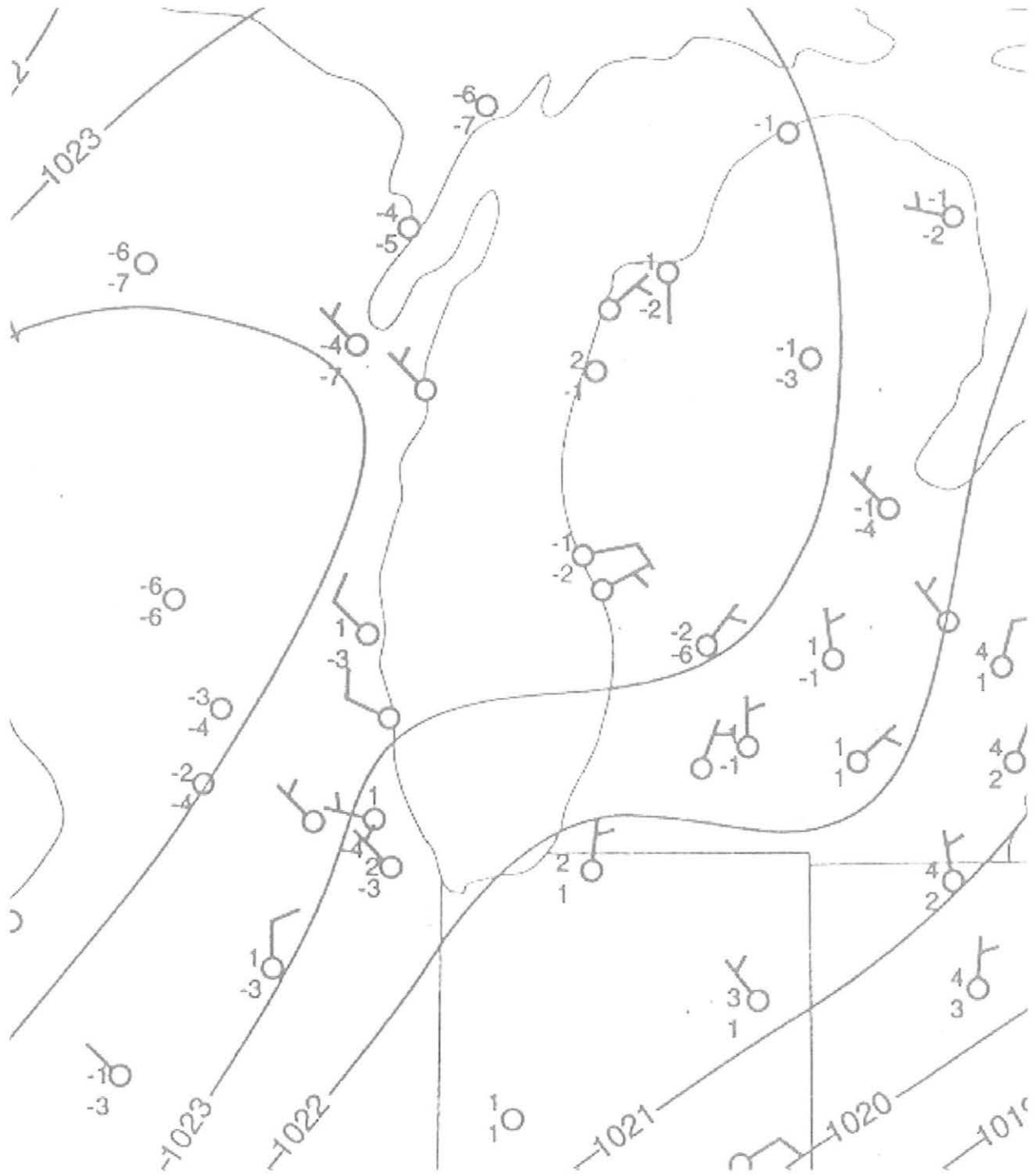


Fig. 3. Surface observations at 1200 UTC 7 November 1978 showing convergence over the lake (After Bader et al. 1995).

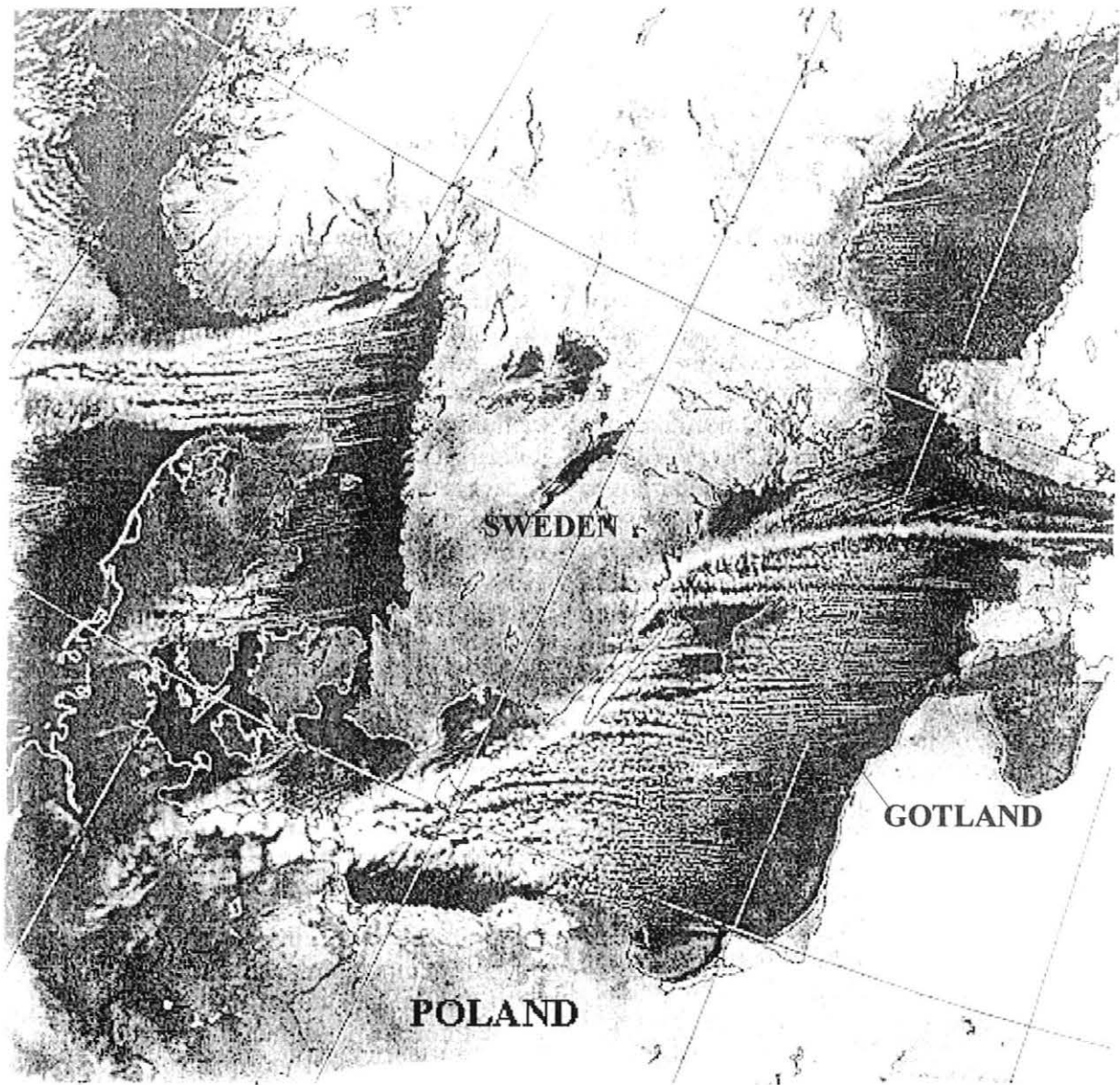


Fig. 4. Infrared satellite imagery at 1235 UTC 11 Jan 1987 showing snow bands over the seas. The gulf band exits the Gulf of Finland and dissipates over eastern Sweden. The corner band begins west of the island of Gotland and continues southwest, merging with the bay band north Poland (After Andersson and Gustafsson 1994).

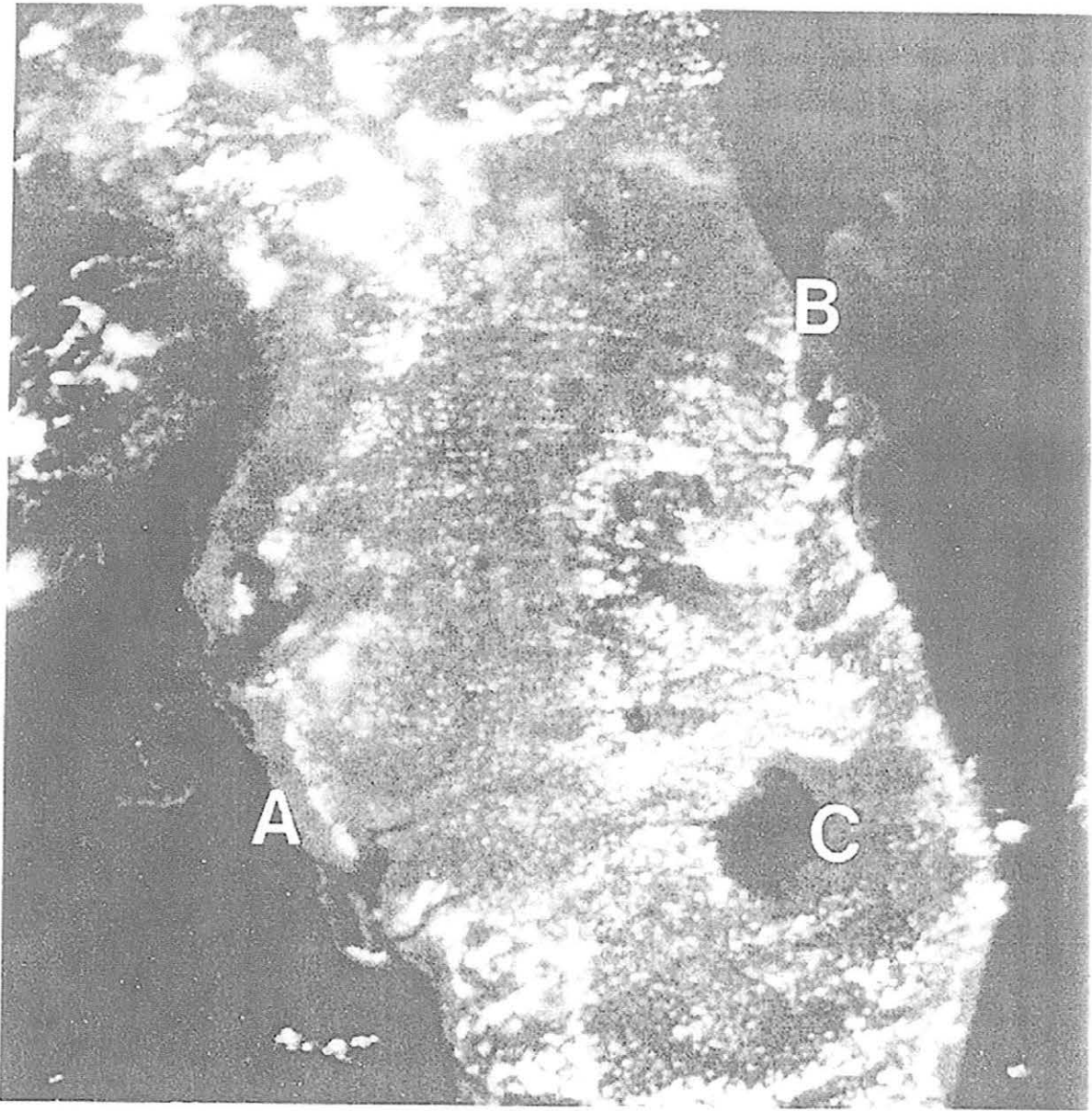


Fig. 5. GOES-7 1 km resolution visible imagery over central Florida at 1600 UTC 18 September 1987. Notice the sea breeze front is adjusted inland on the west coast and closer to the coastline on the east coast due to the mean westerly flow (After Bader et al. 1995).

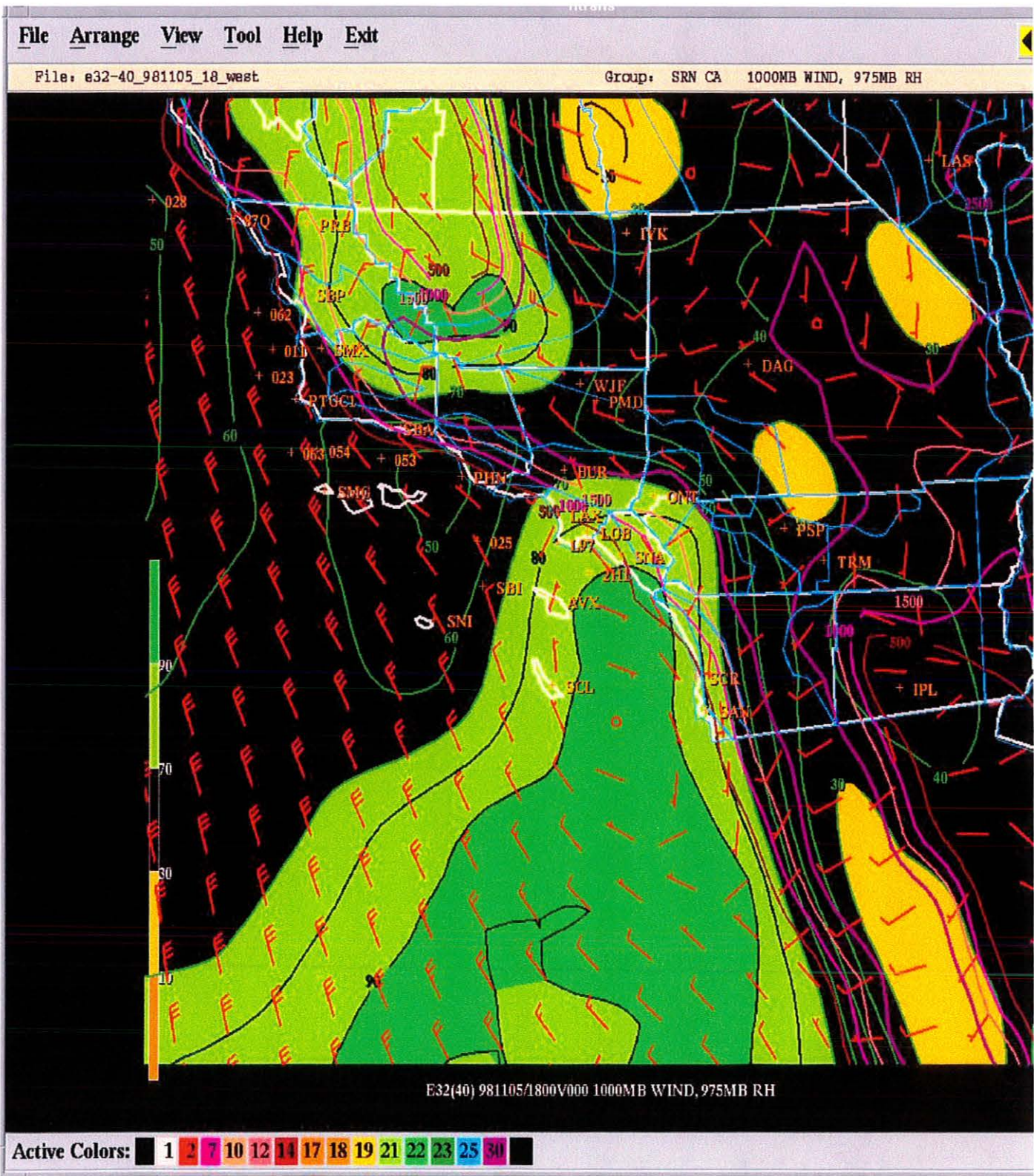


Fig. 6. 1800 UTC 5 November 1998 32 km ETA 1000 MB wind and 975 MB RH indicating a Catalina Eddy.

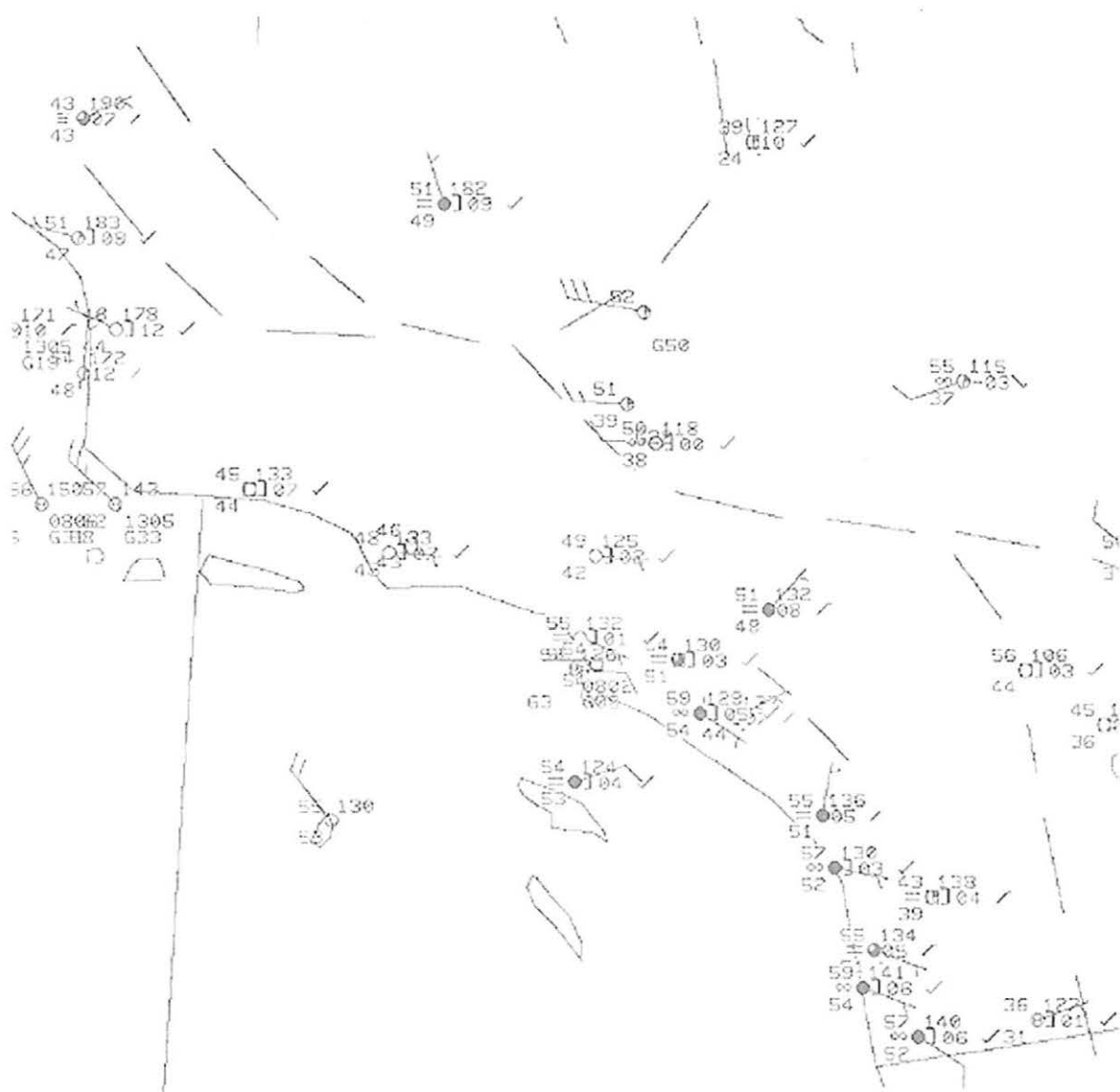


Fig. 7. 1500 UTC 5 November 1998 surface plot. The dashed lines indicate the ridge lines of the higher mountain ranges.

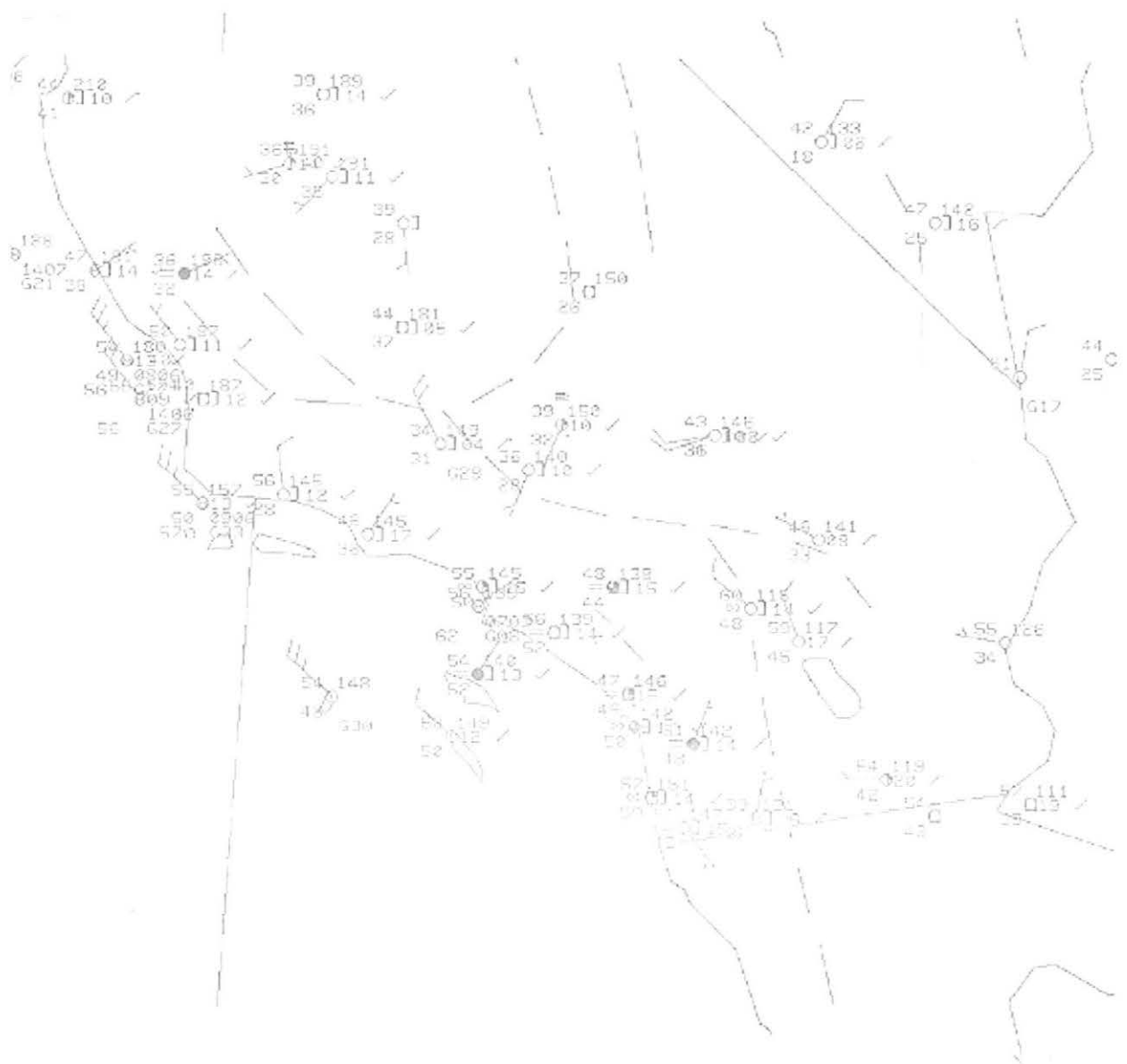


Fig. 8. 1500 UTC 6 November 1998 surface plot. The dashed lines indicate the ridge lines of the higher mountain ranges.

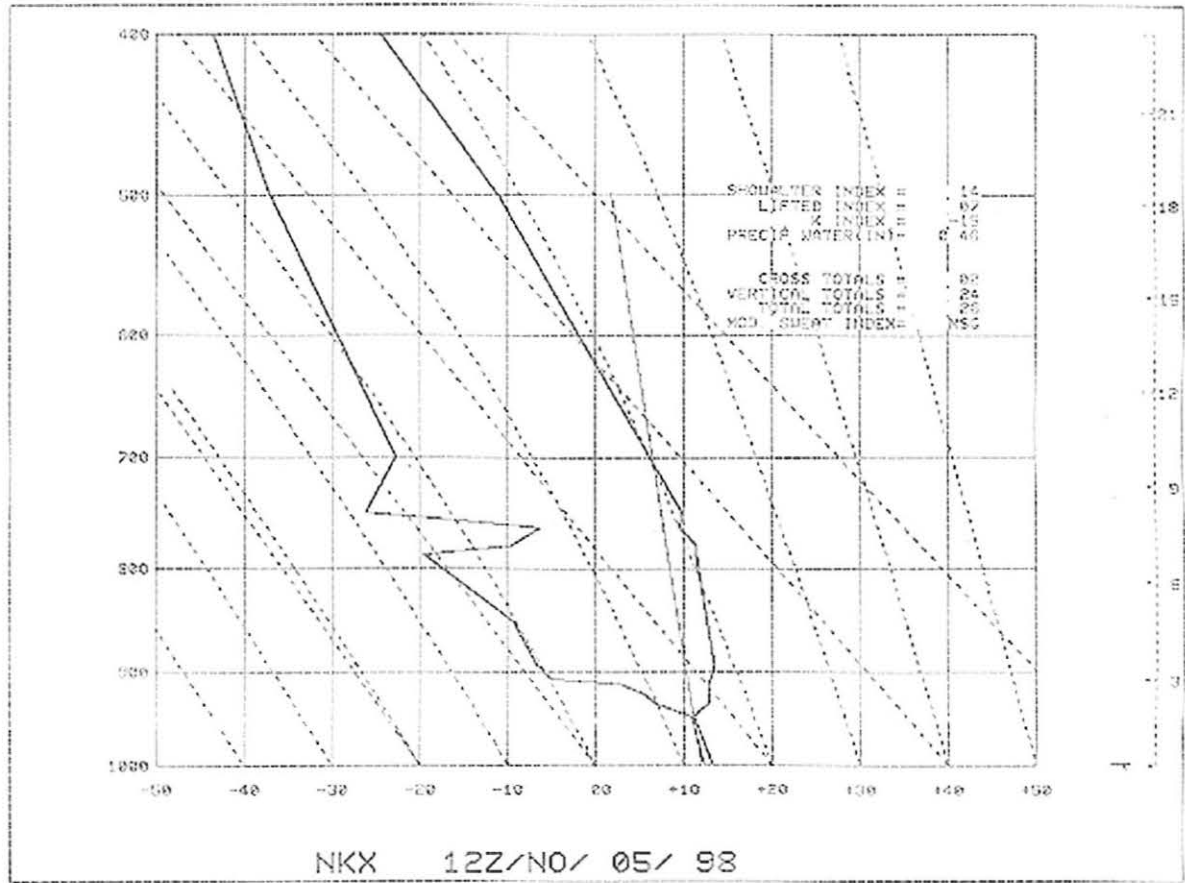


Fig. 9. 1200 UTC 5 November 1998 NKX raob.

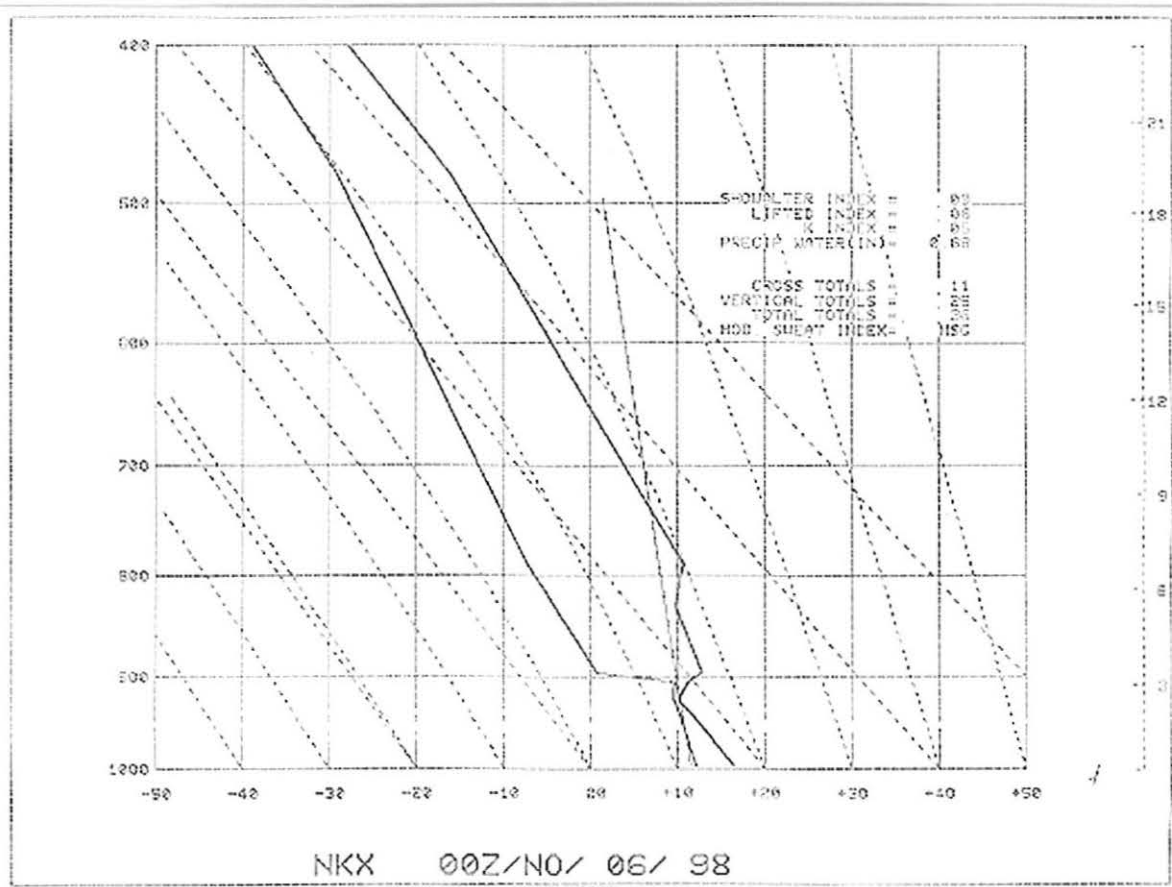


Fig. 10. 0000 UTC 6 November 1998 NKX raob.

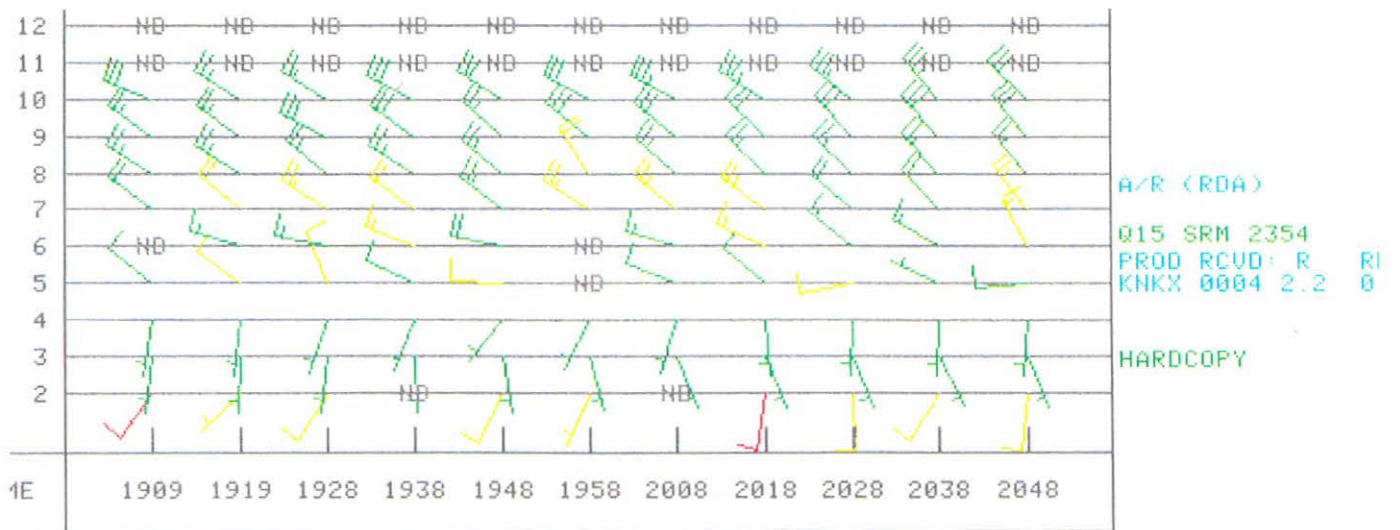


Fig. 11. 2048 UTC 5 November 1998 KNKX VAD wind profile.

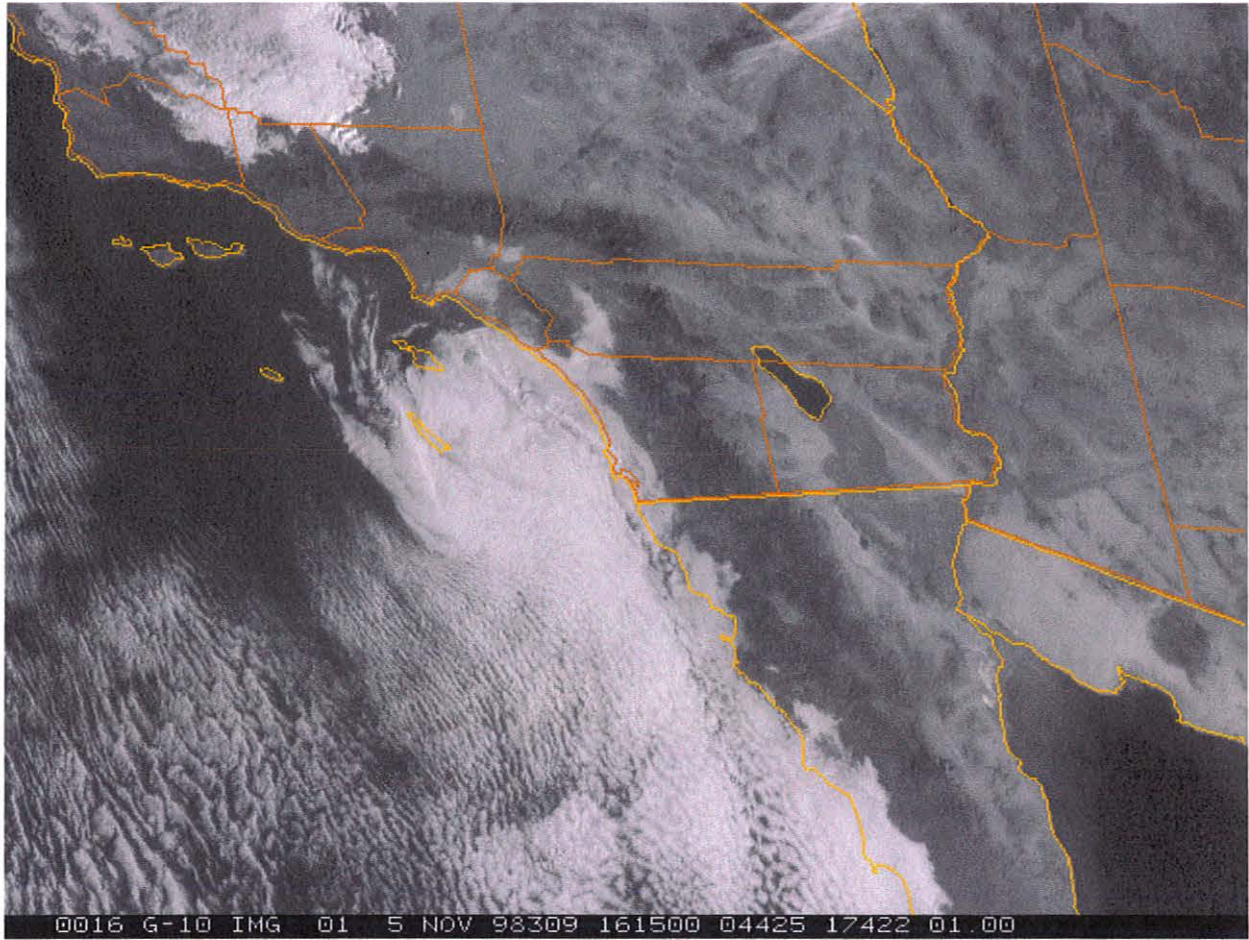


Fig. 12. 1615 UTC 5 November 1998 1 km visible satellite imagery.

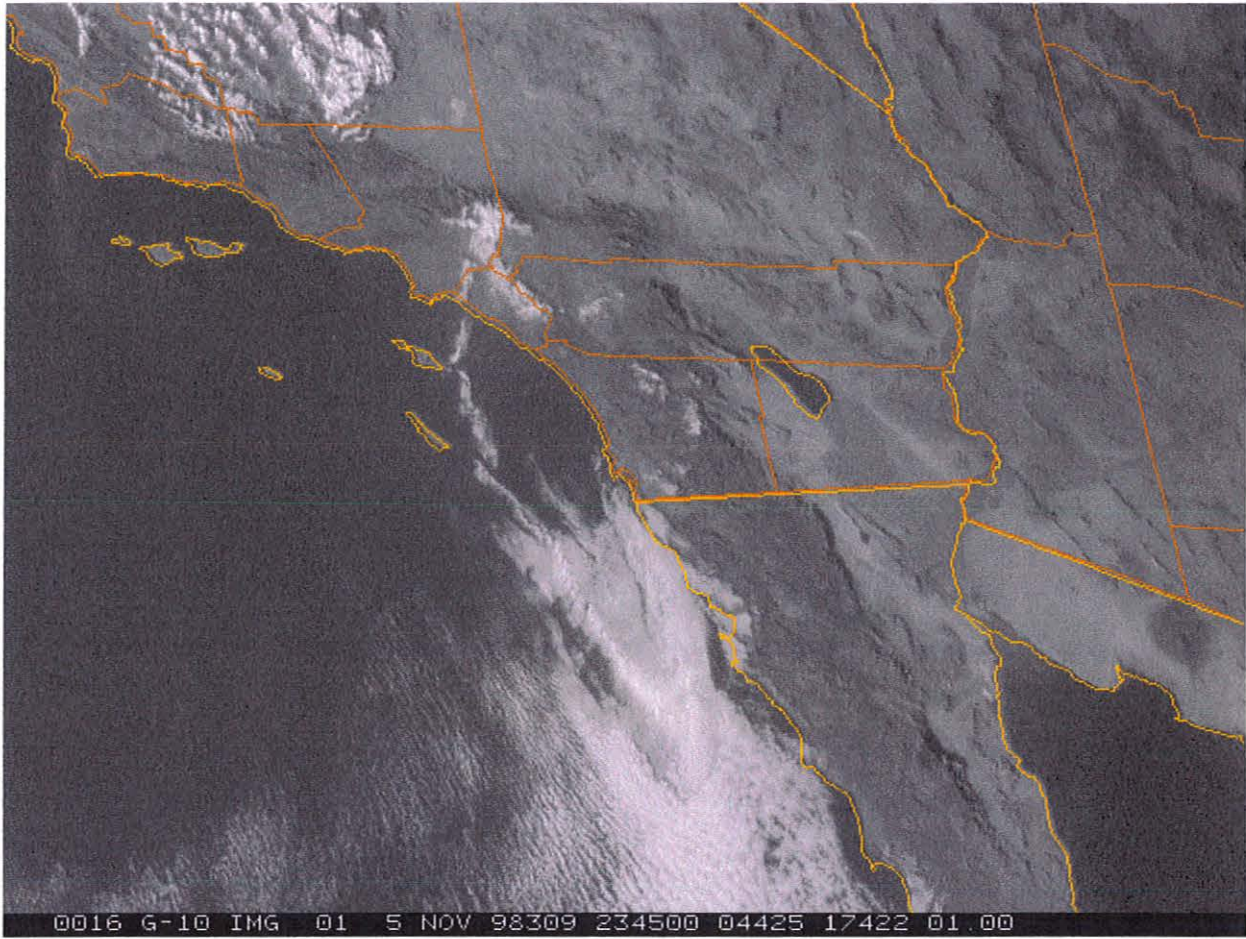


Fig. 13. 2345 UTC 5 November 1998 1 km visible satellite imagery.

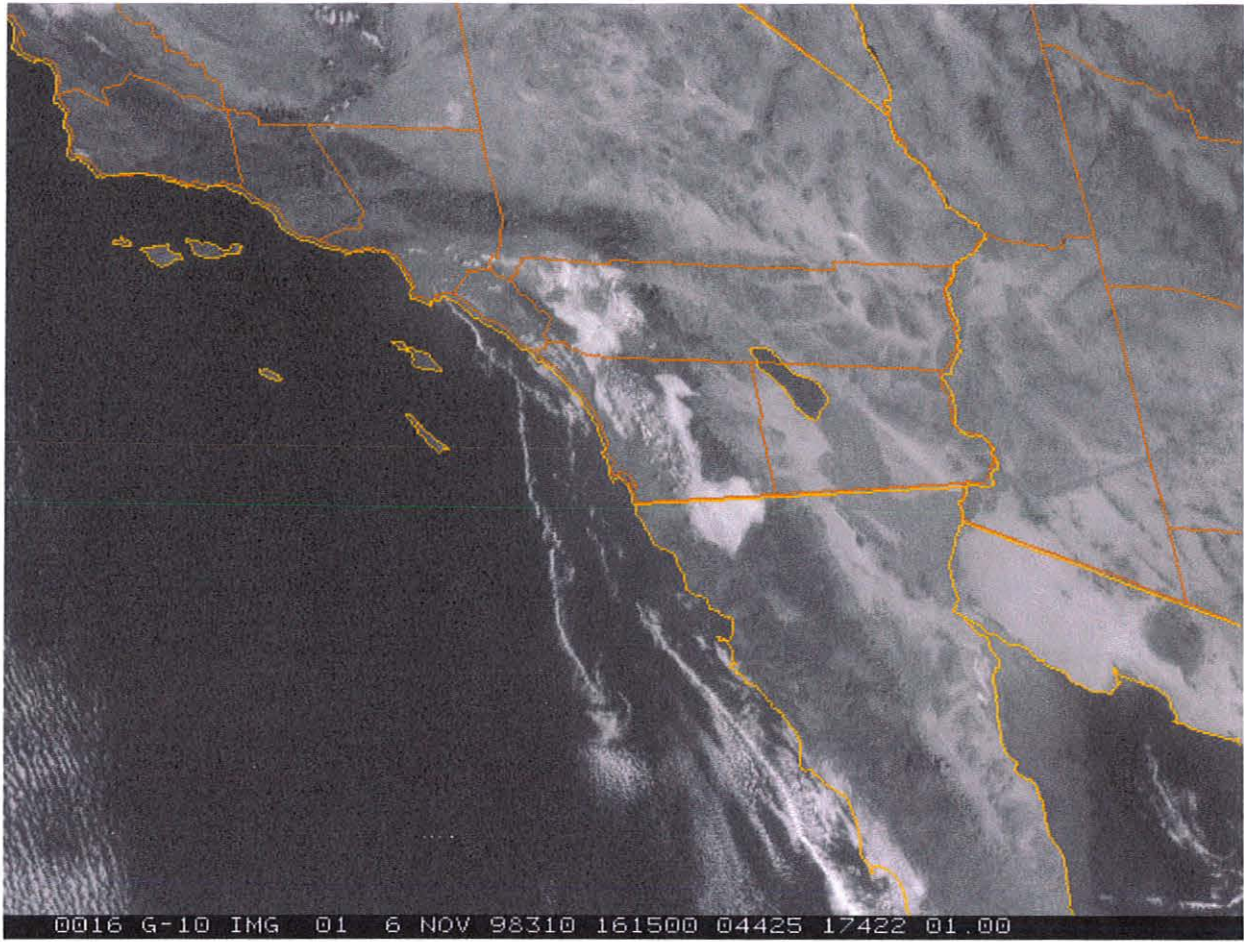


Fig. 14. 1615 UTC 6 November 1998 1 km visible satellite imagery.

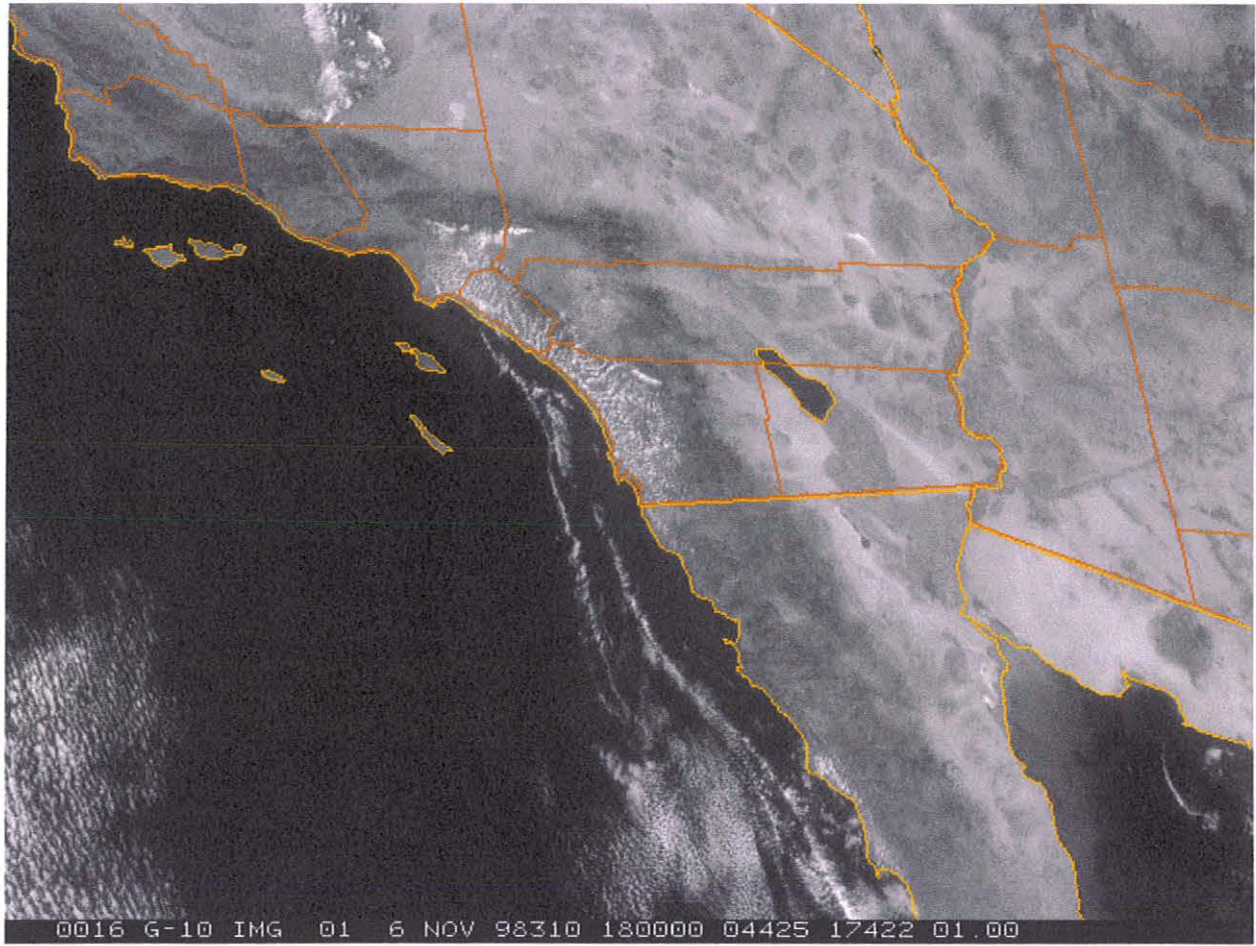


Fig. 15. 1800 UTC 6 November 1998 1 km visible satellite imagery.

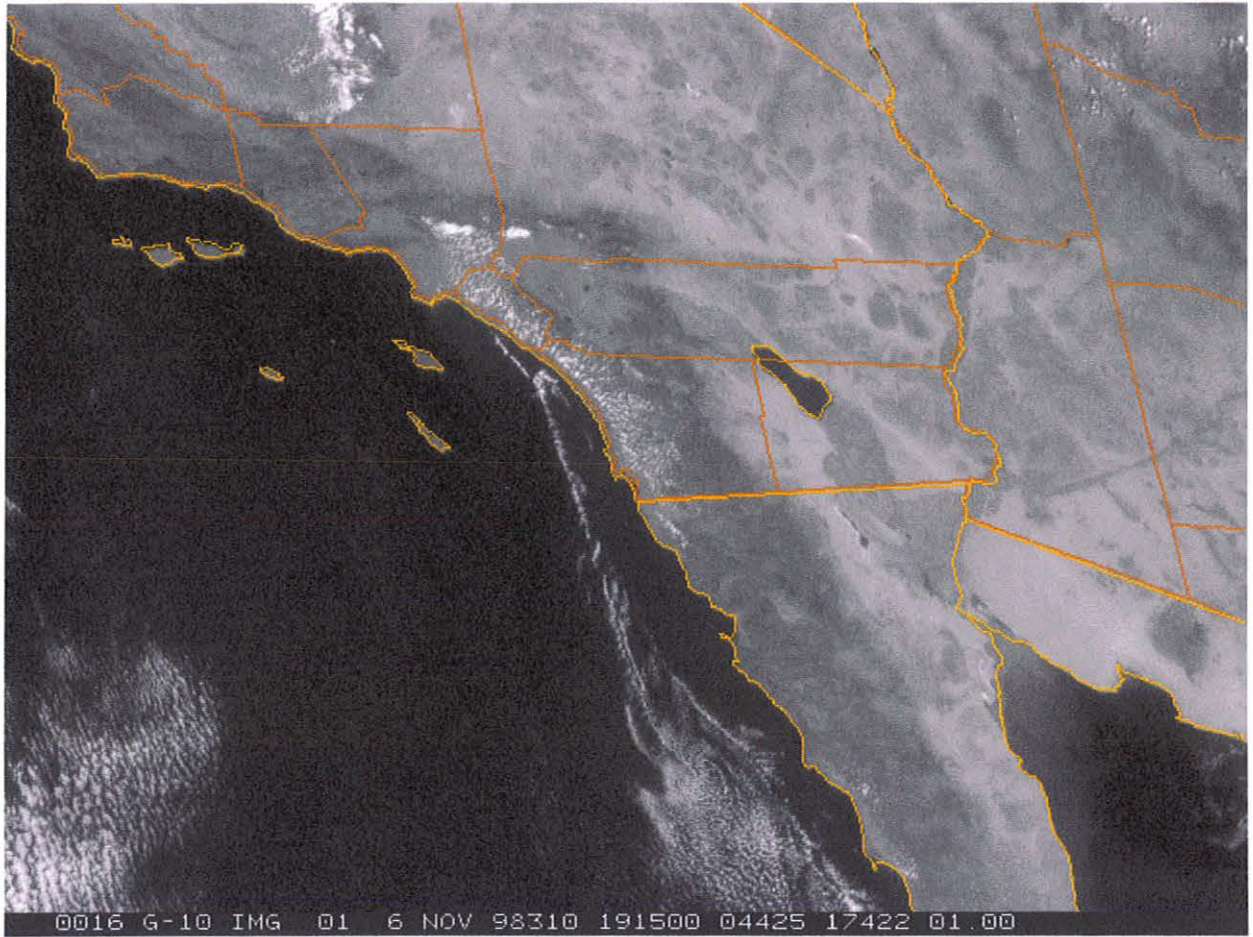


Fig. 16. 1915 UTC 6 November 1998 1 km visible satellite imagery.

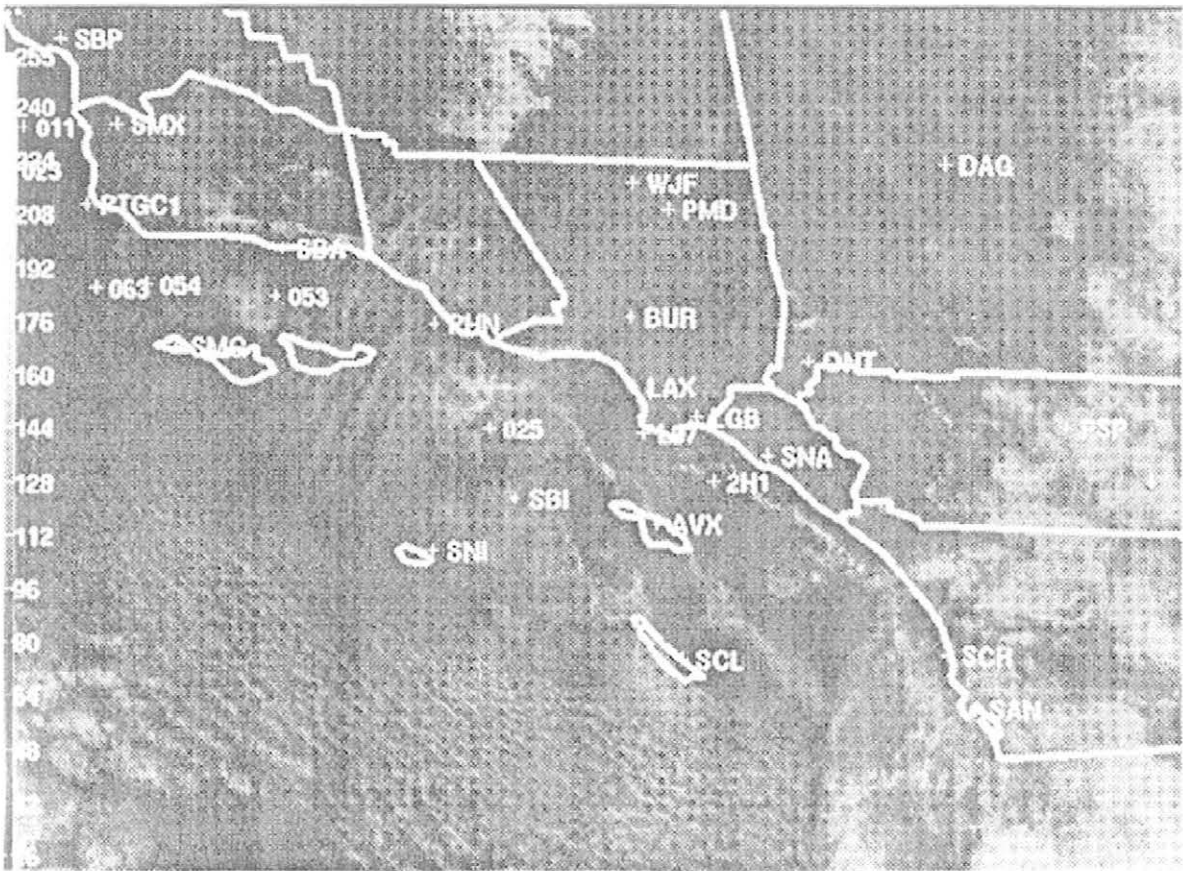


Fig. 17. 1800 UTC 20 May 1998 1 km visible satellite imagery (After Martin 1998).

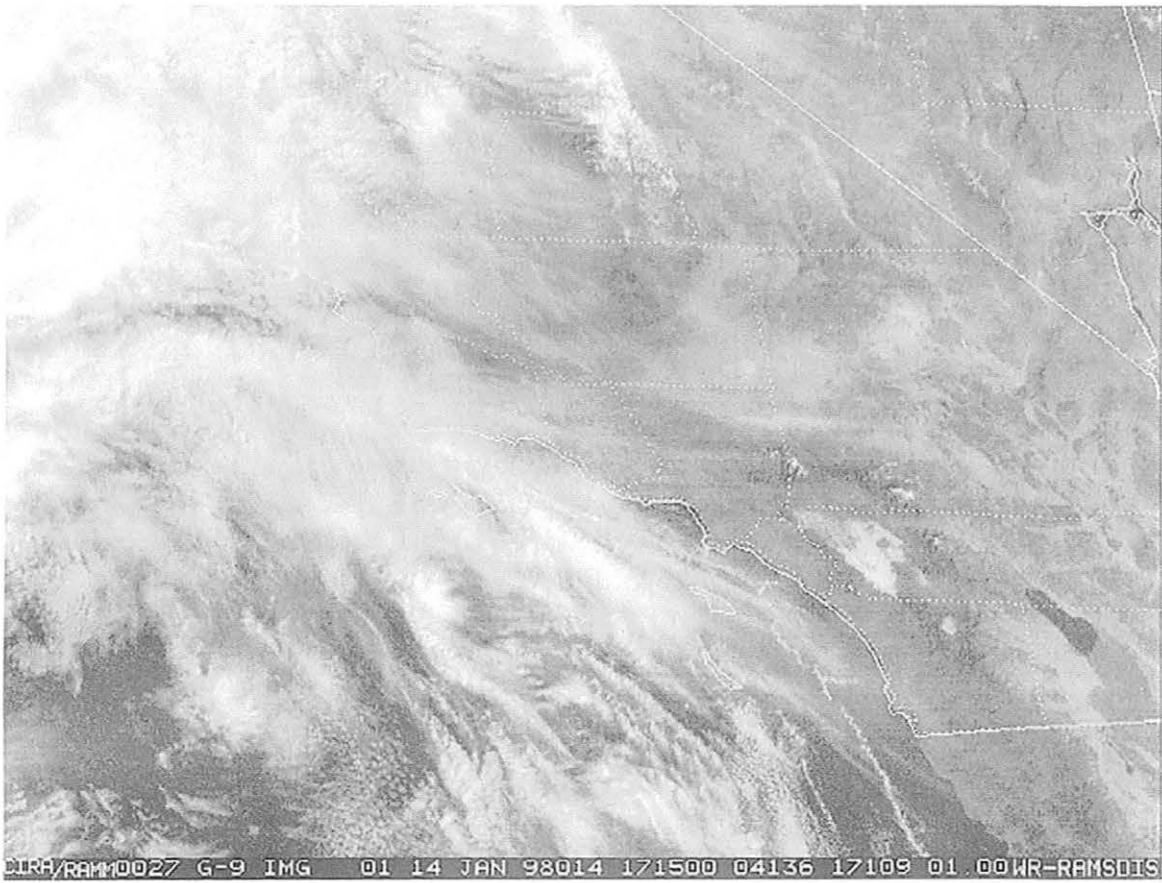


Fig. 18. 1715 UTC 14 January 1998 1 km visible satellite imagery.

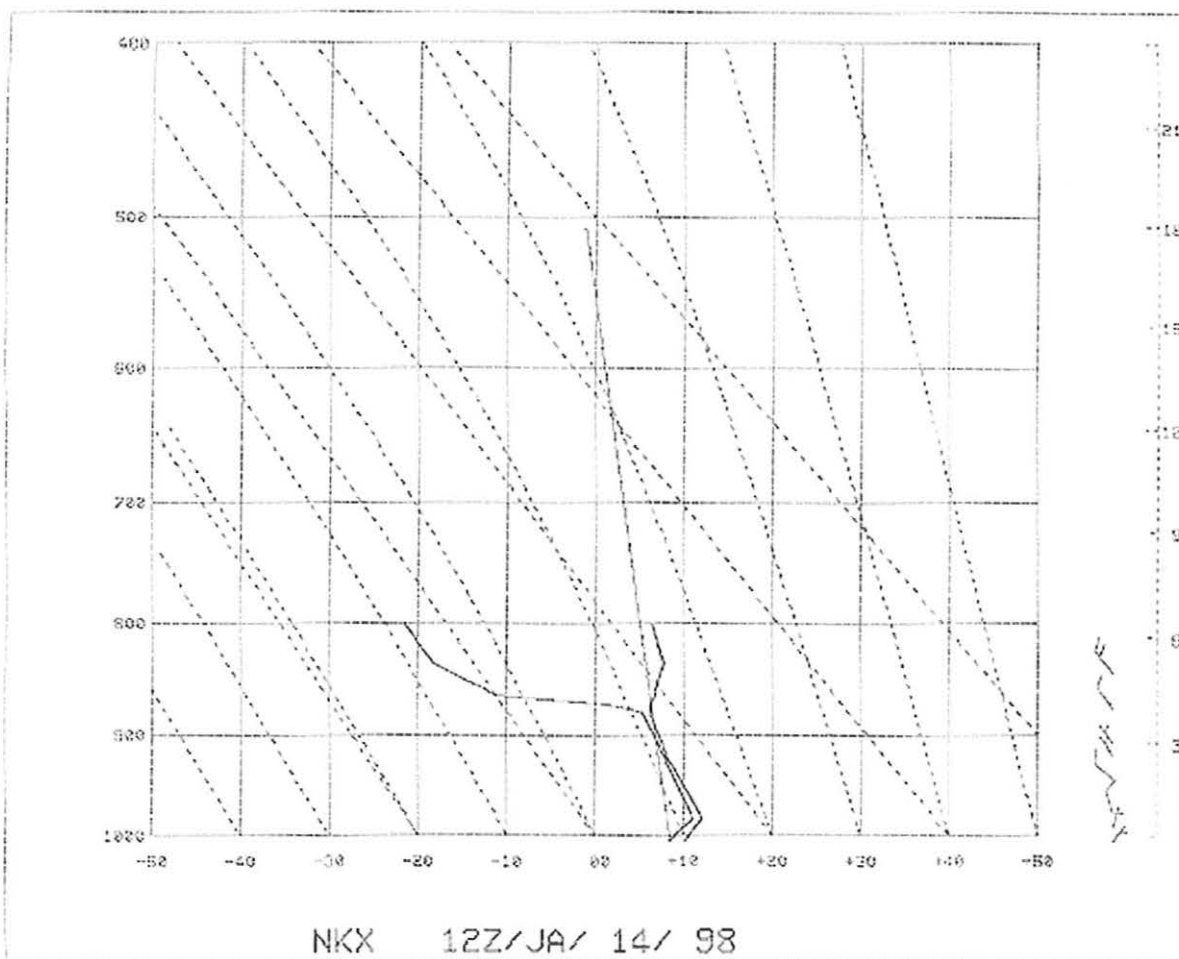


Fig. 19. 1200 UTC 14 January 1998 NKX raob.

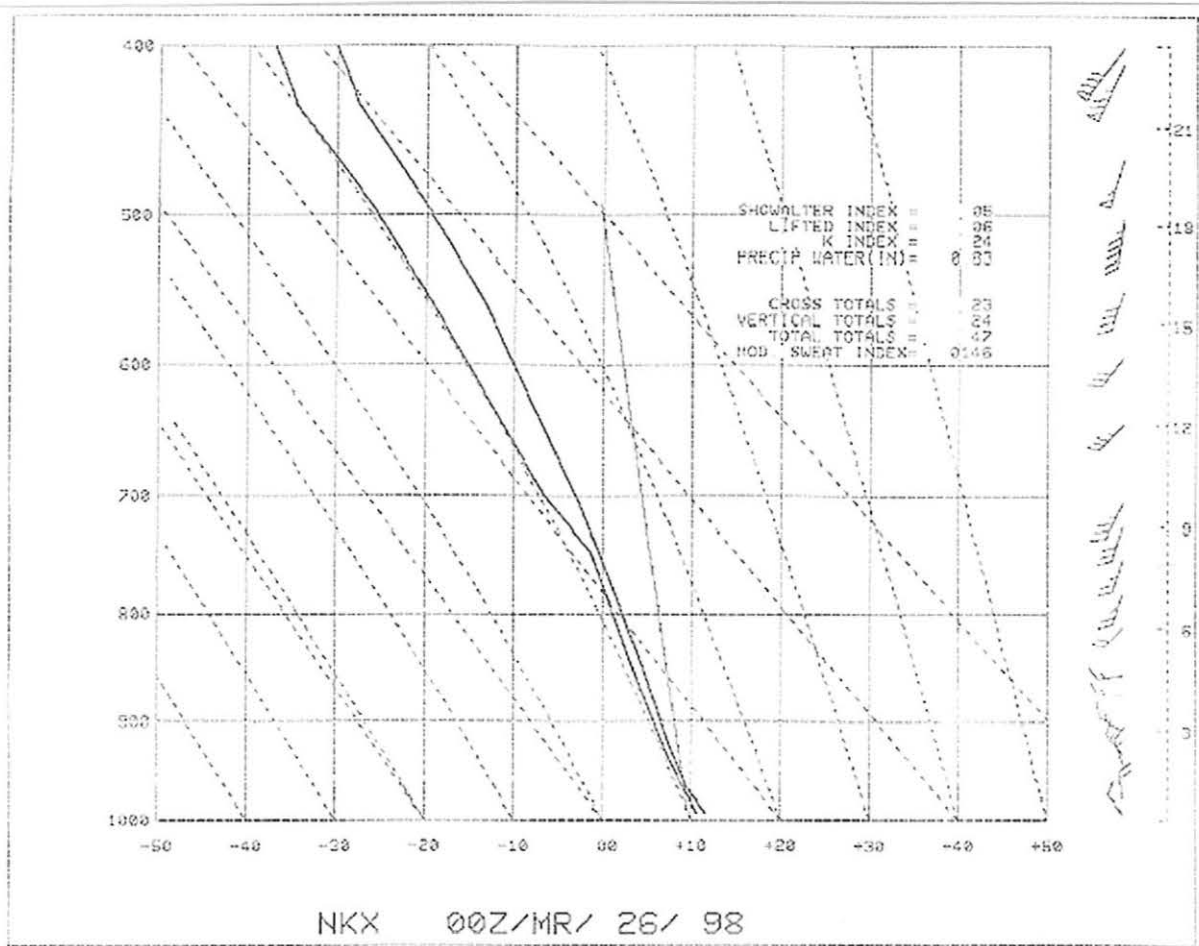


Fig. 20. 0000 UTC 26 March 1998 NKX raob.

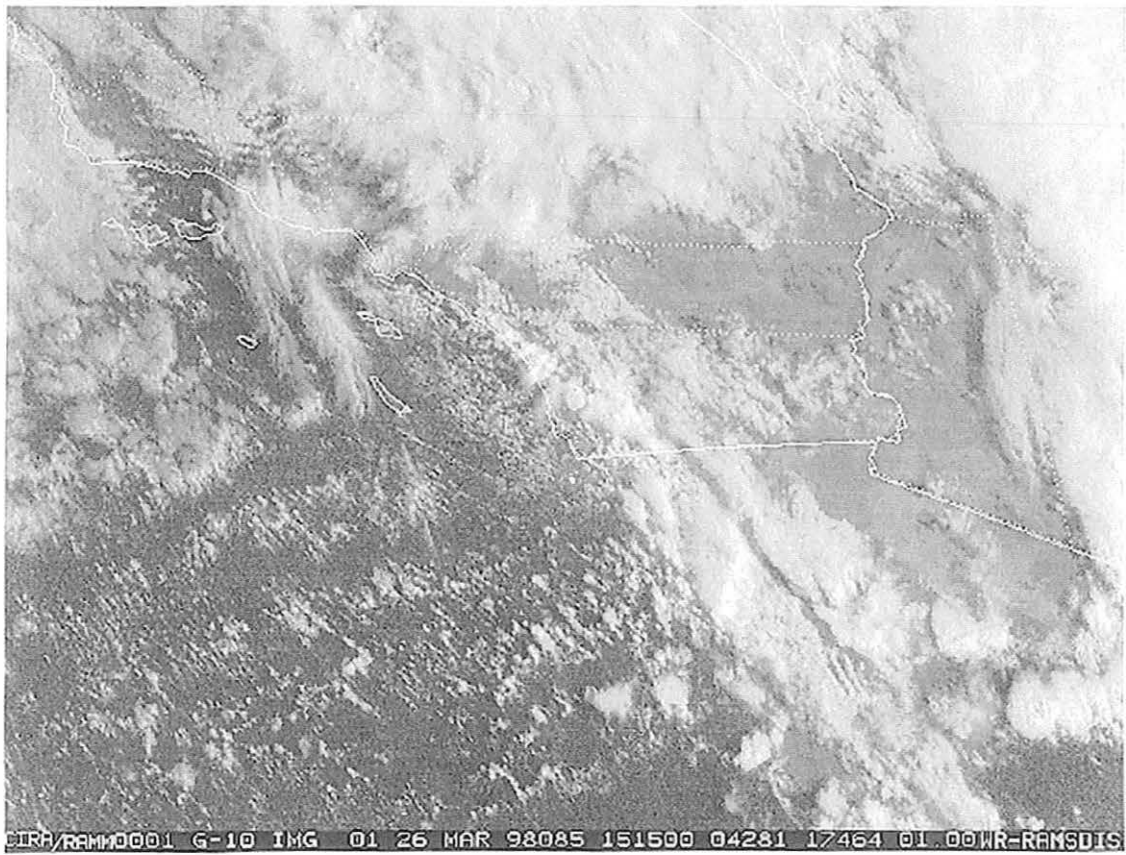


Fig. 21. 1515 UTC 26 March 1998 1 km visible satellite imagery.

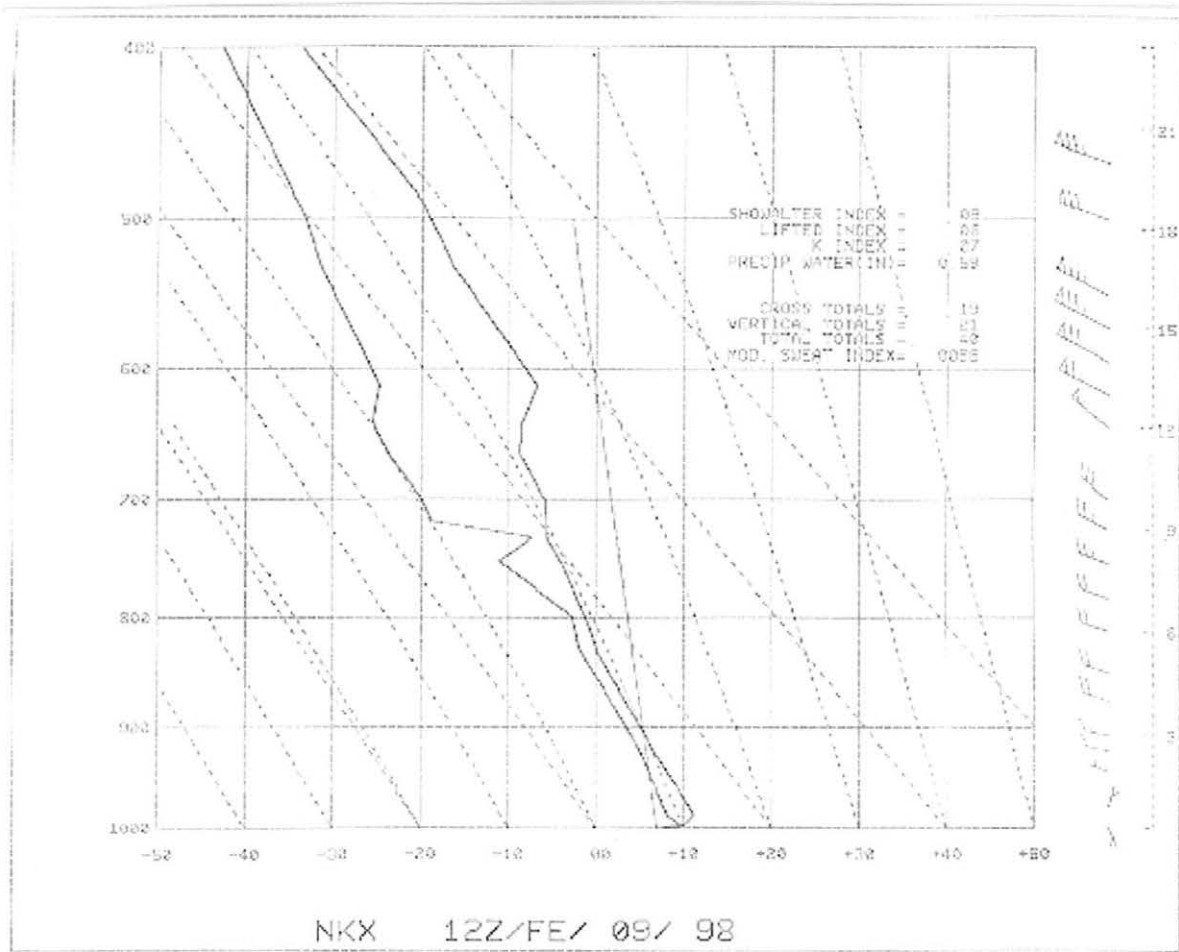


Fig. 22. 1200 UTC 9 February 1998 NKX raob.

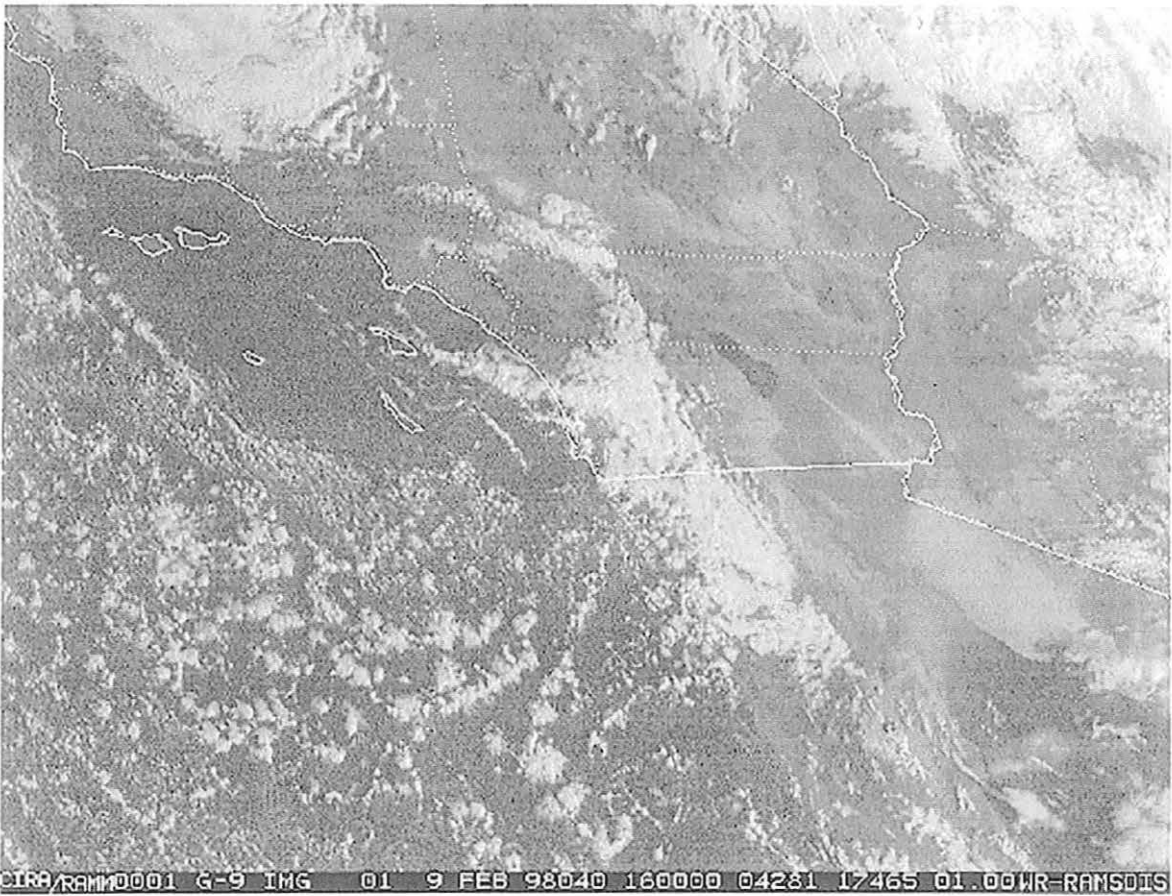


Fig. 23. 1600 UTC 9 February 1998 1 km visible satellite imagery.

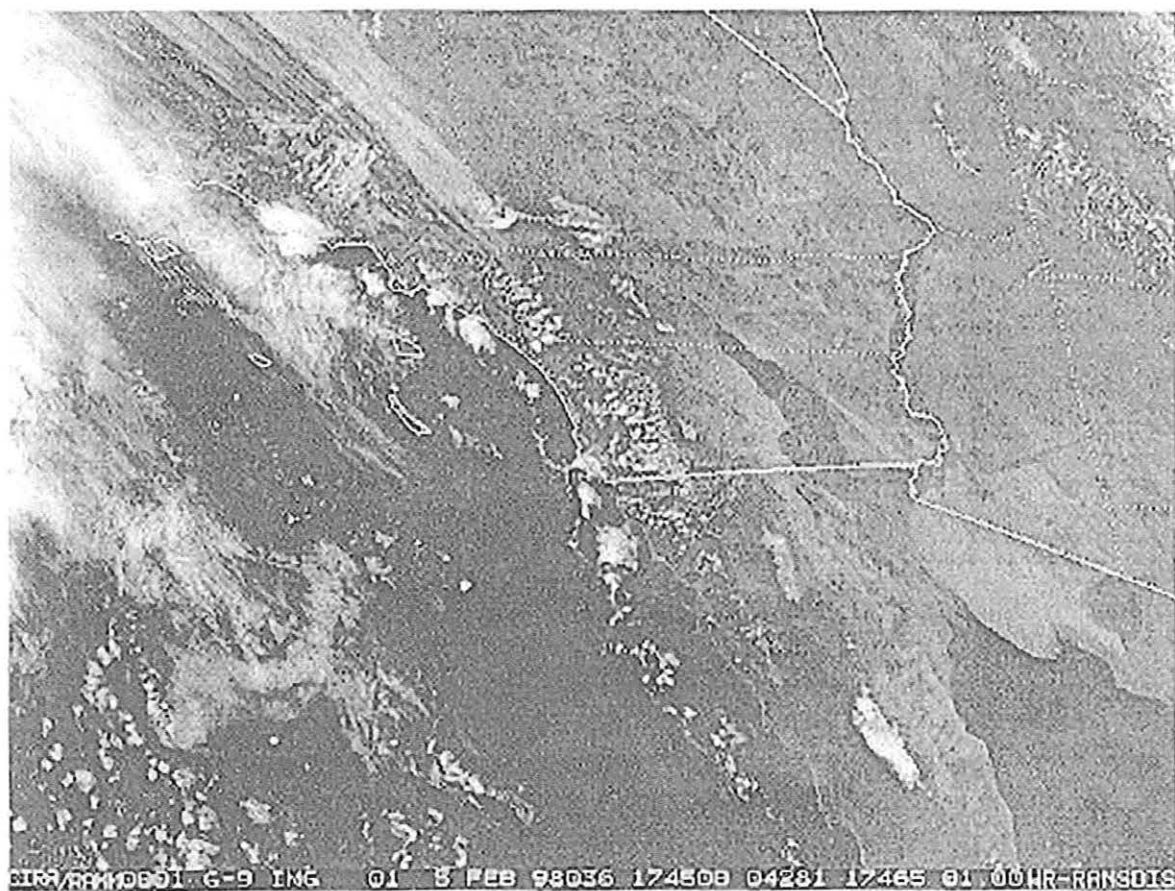


Fig. 24. 1745 UTC 5 February 1998 1 km visible satellite imagery.

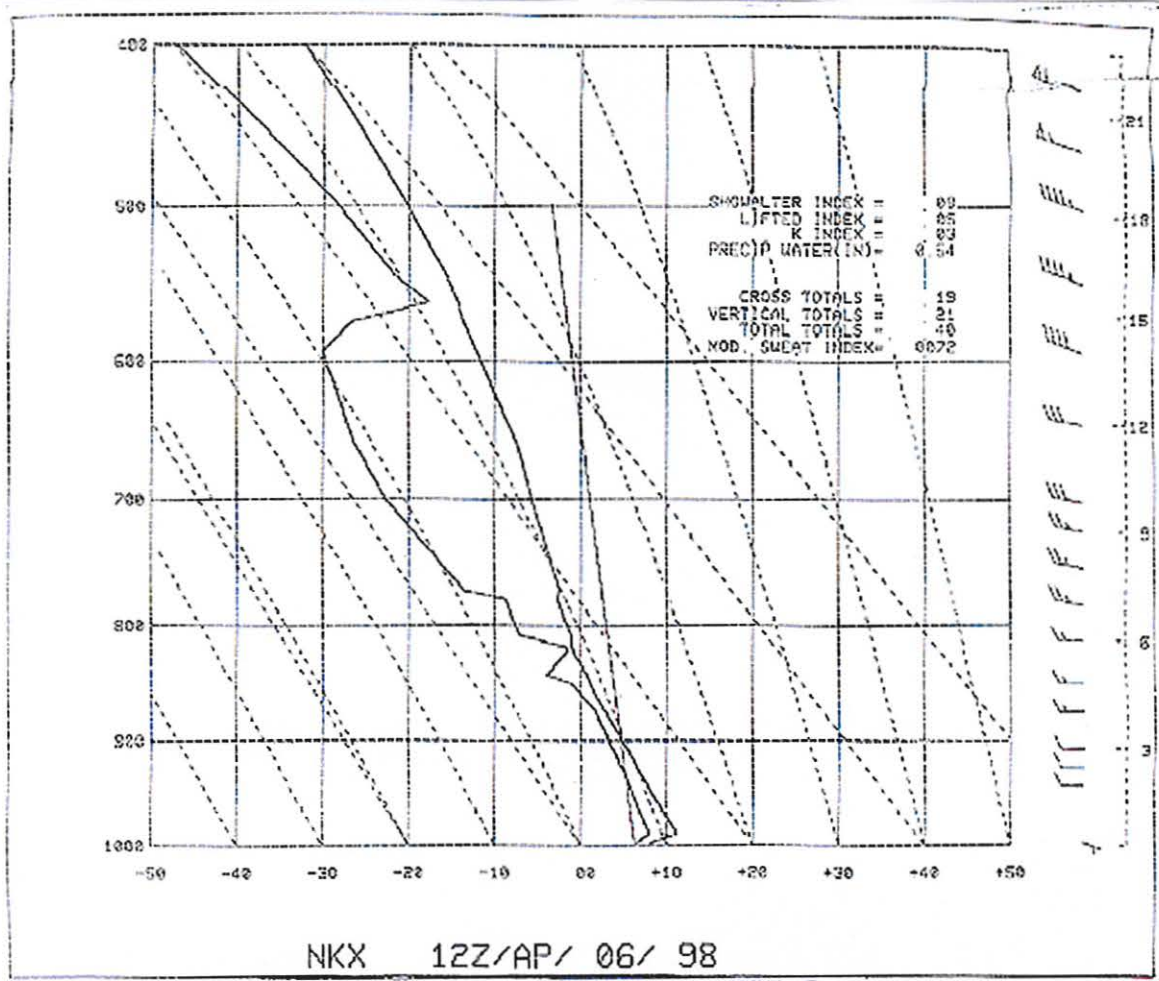


Fig. 25. 1200 UTC 6 April 1998 NKX raob.

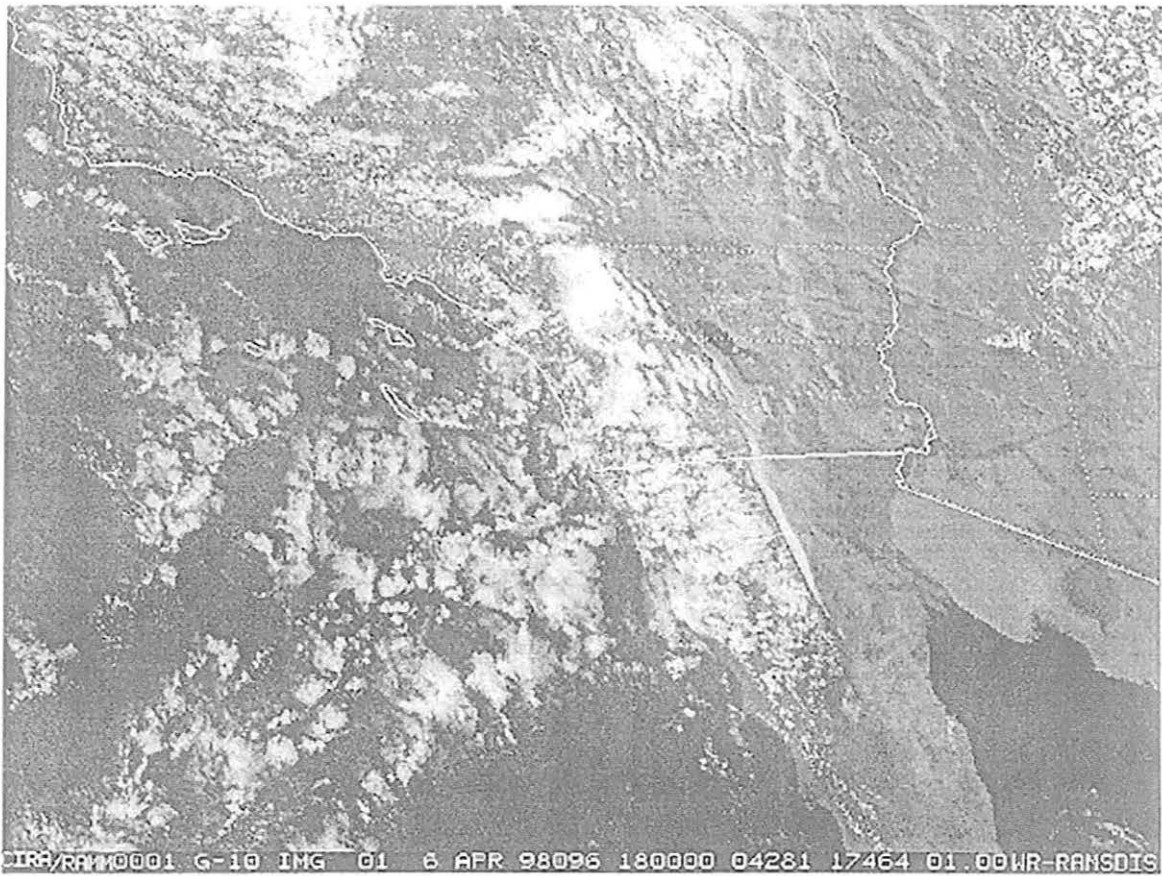


Fig. 26. 1800 UTC 6 April 1998 1 km visible satellite imagery.

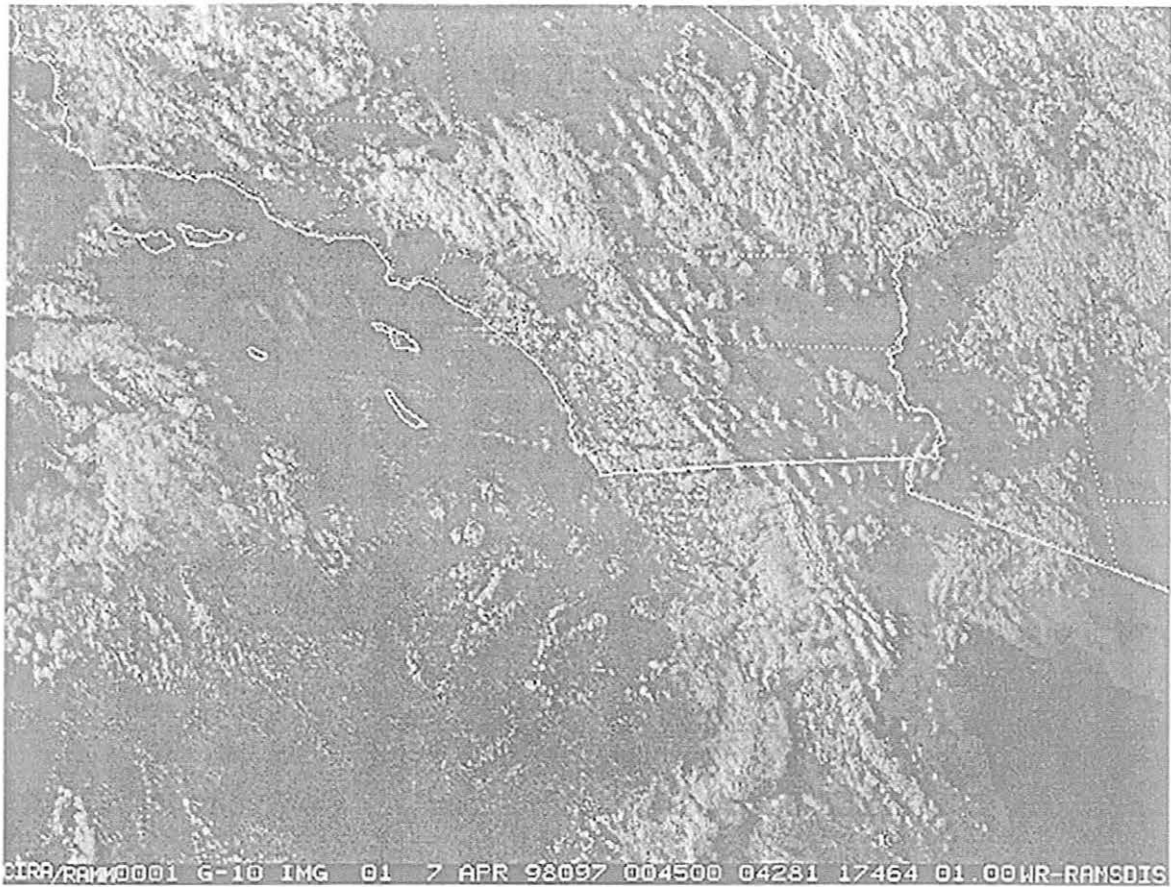


Fig. 27. 0045 UTC 7 April 1998 1 km visible satellite imagery.

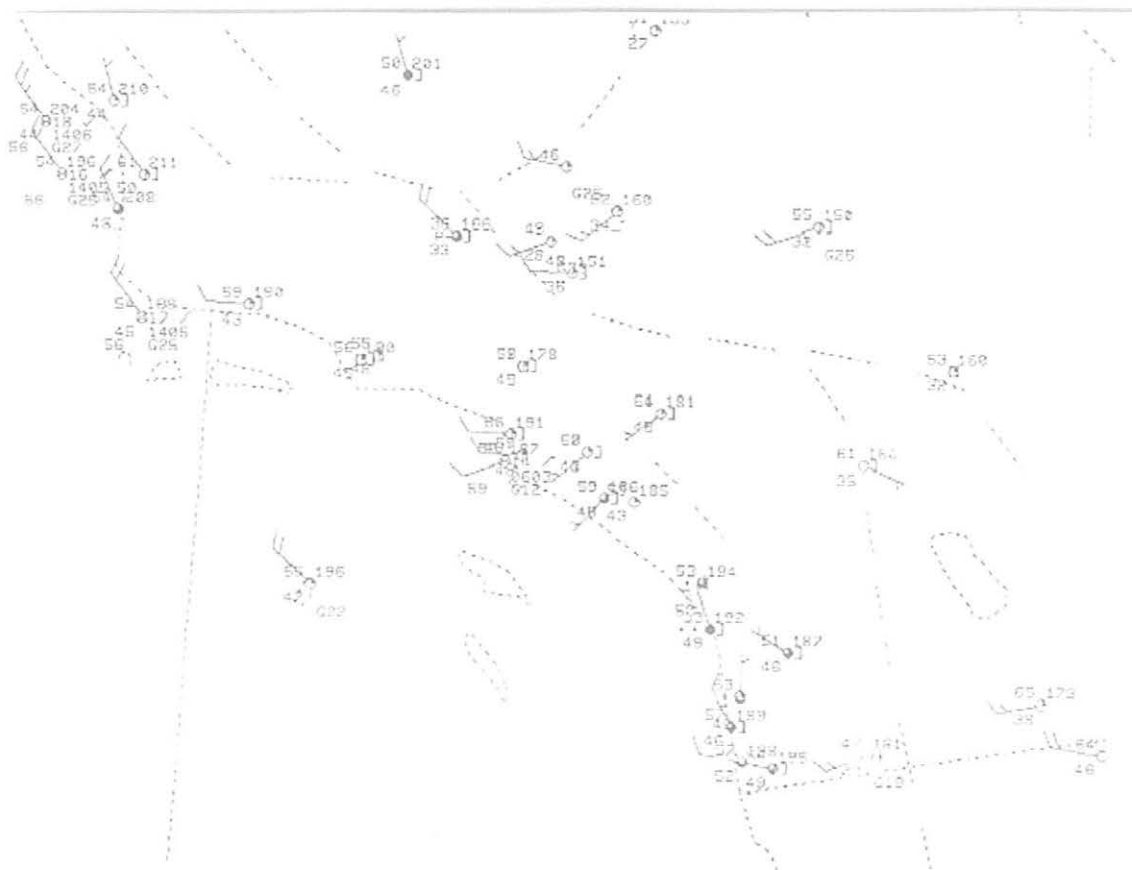


Fig. 29. 1700 UTC 7 April 1998 surface plot.

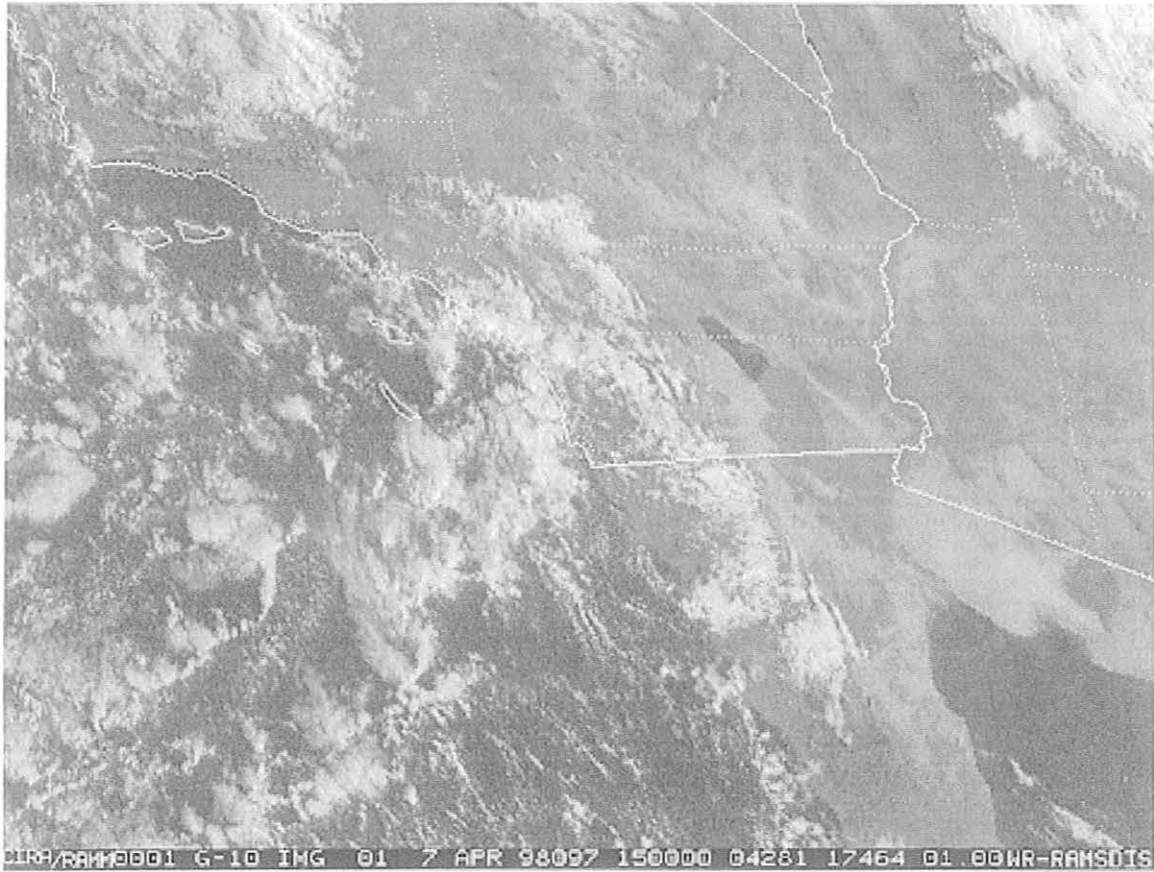


Fig. 30. 1500 UTC 7 April 1998 1 km visible satellite imagery.

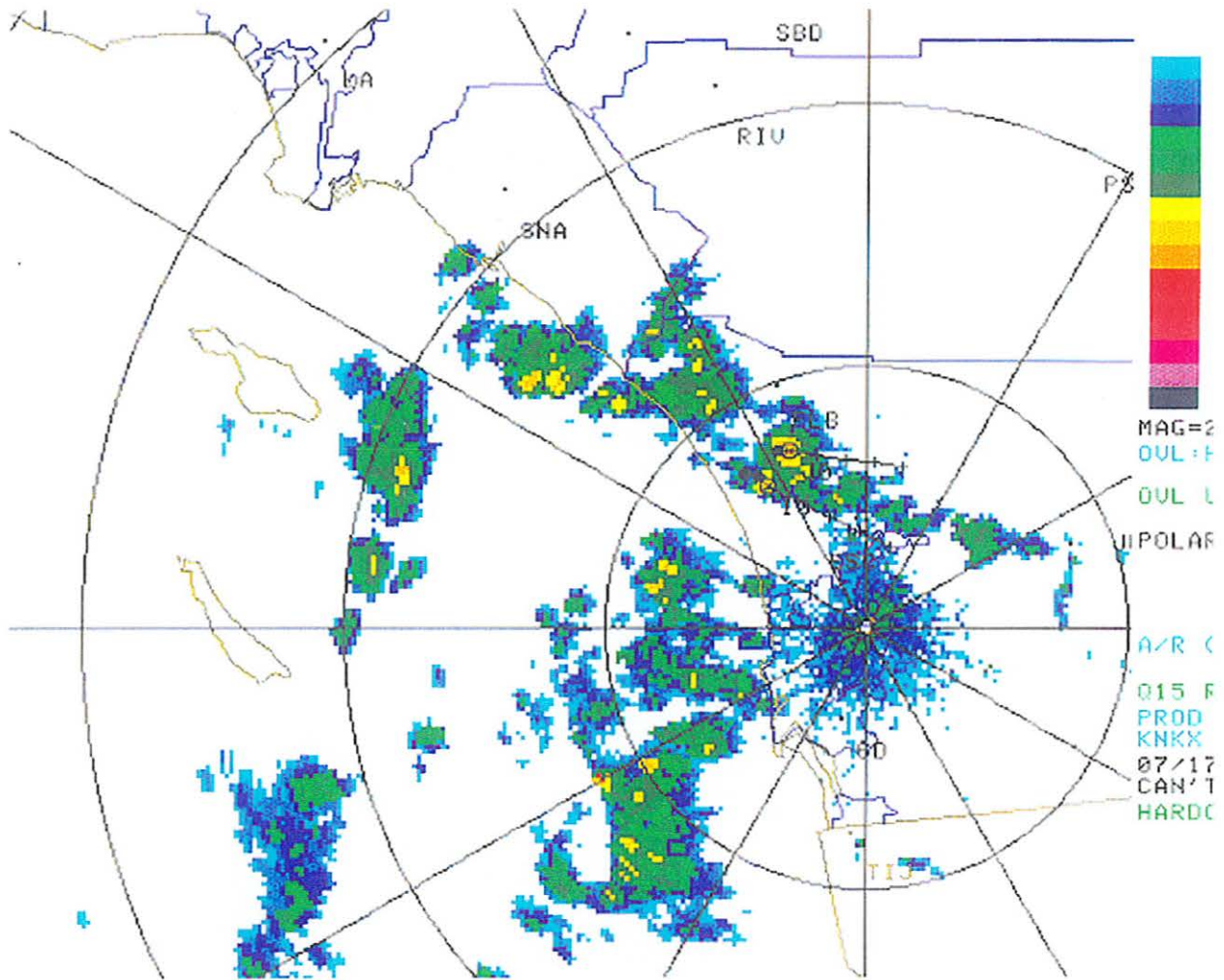


Fig. 31. 1456 UTC 7 April 1998 KNKX composite reflectivity.

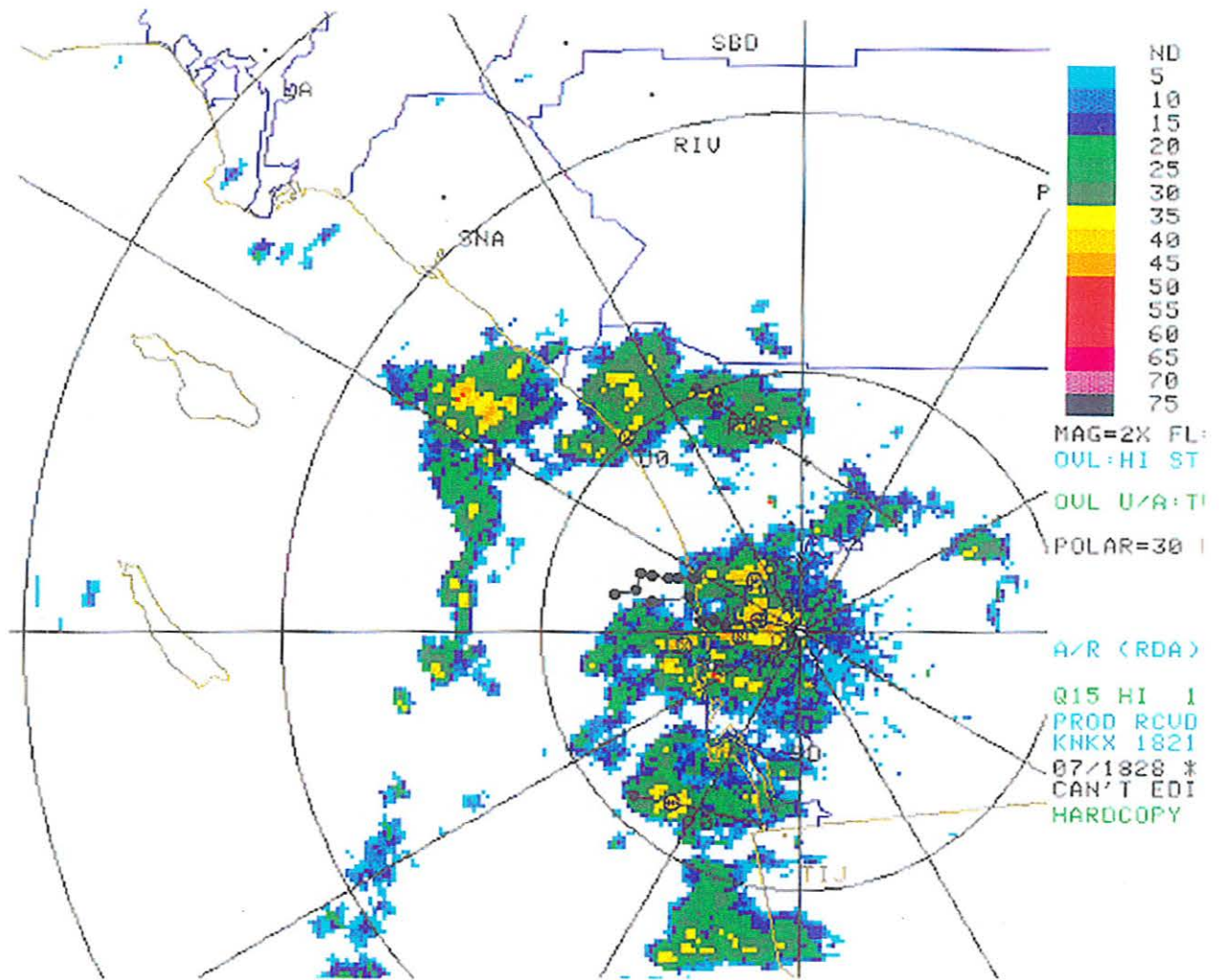


Fig. 32. 1543 UTC 7 April 1998 KNKX composite reflectivity.

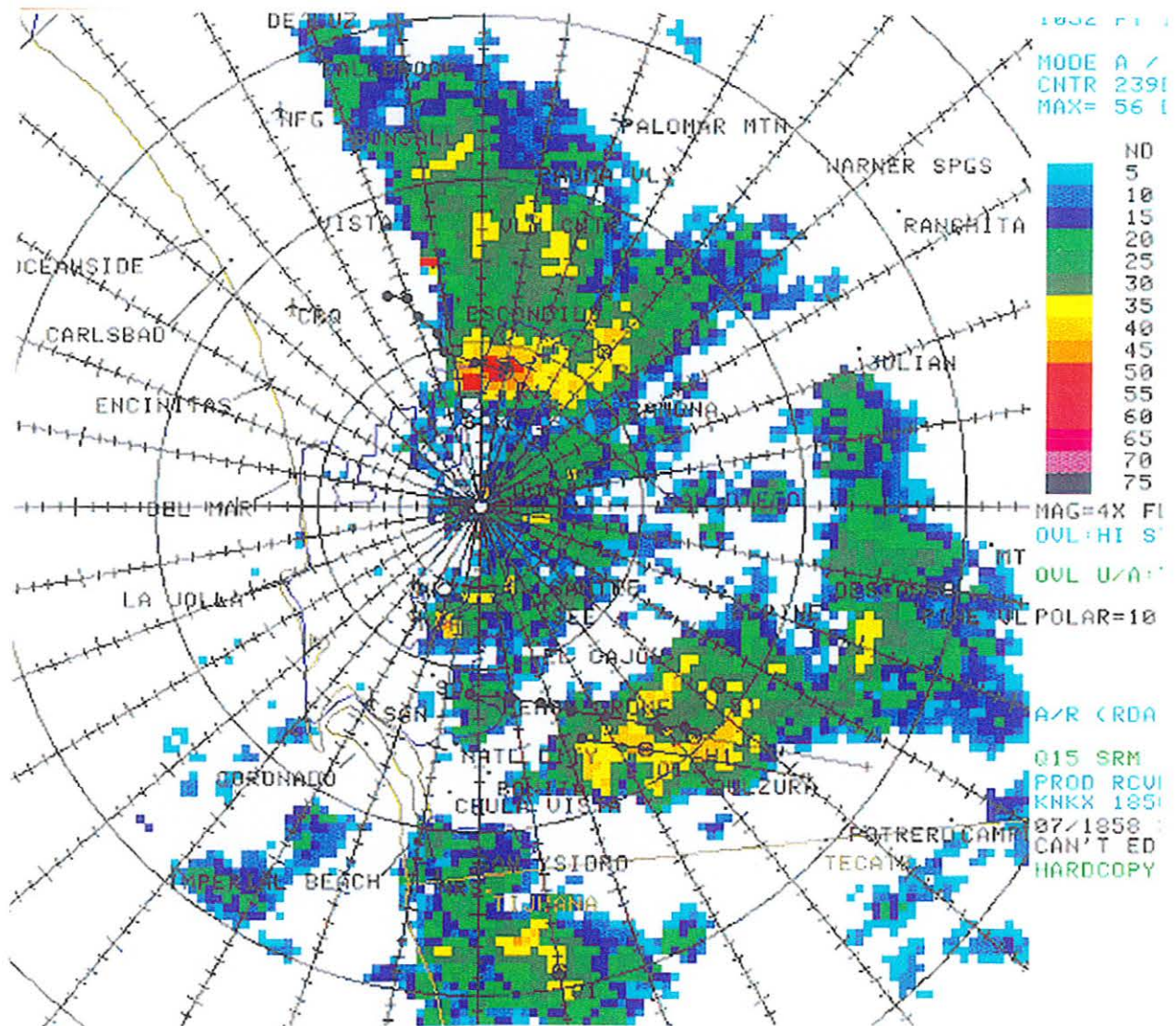


Fig. 33. 1734 UTC 7 April 1998 KNKX composite reflectivity.

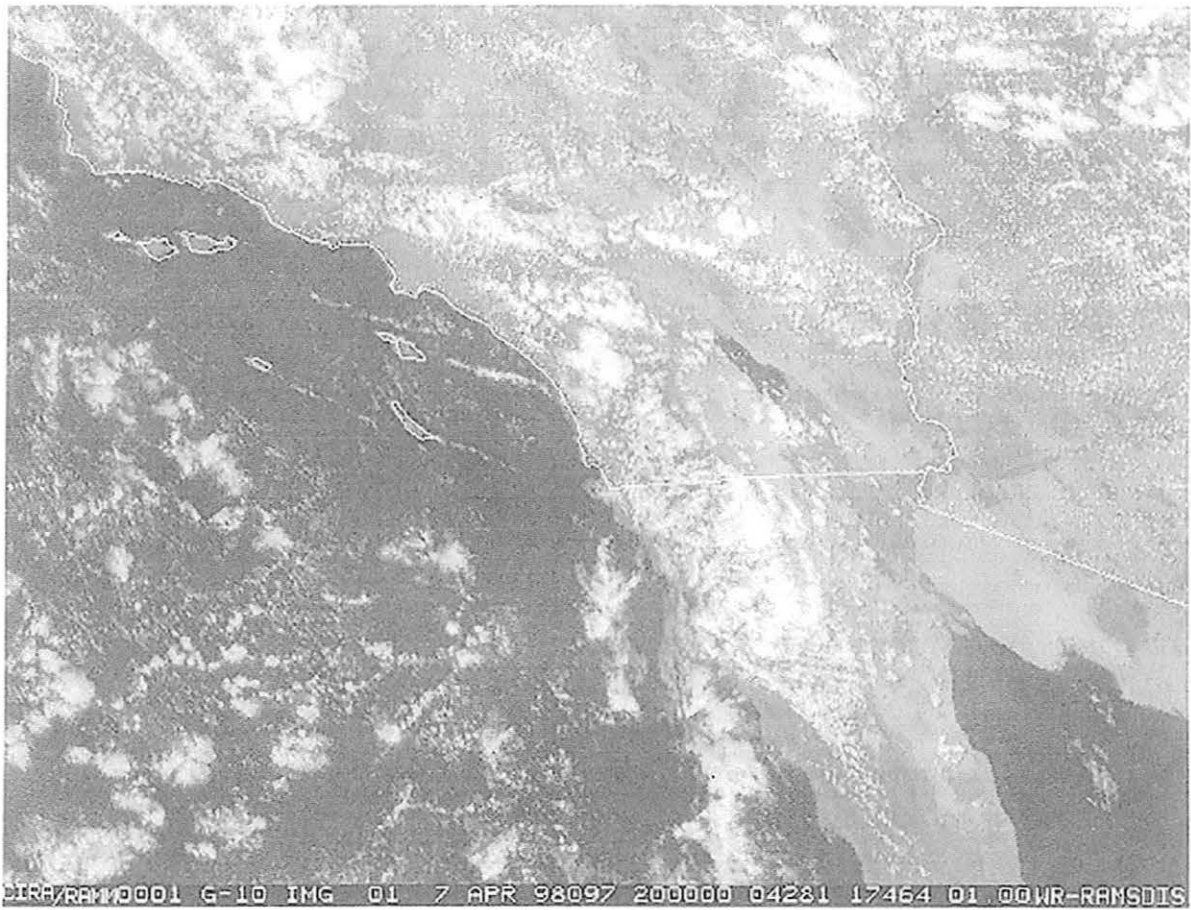


Fig. 34. 2000 UTC 7 April 1998 1 km visible satellite imagery.

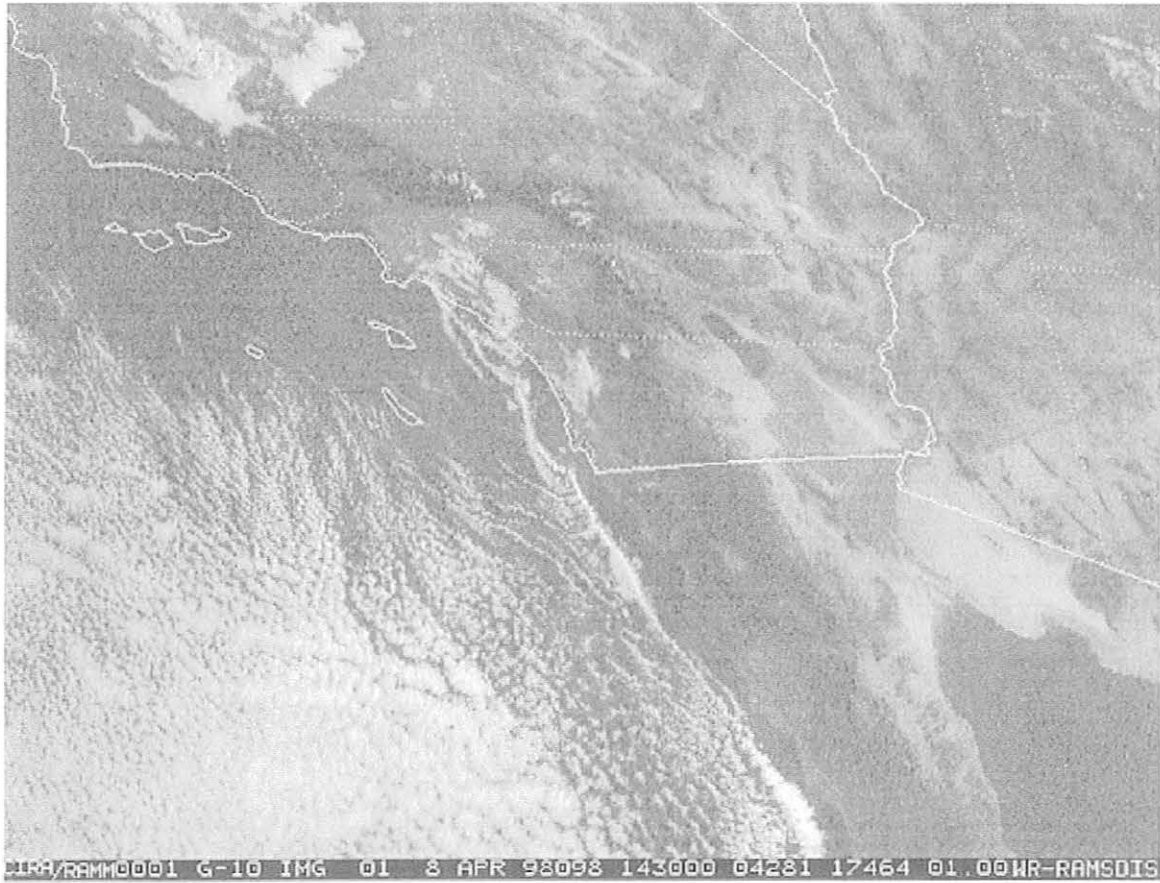


Fig. 35. 1430 UTC 8 April 1998 1 km visible satellite imagery.

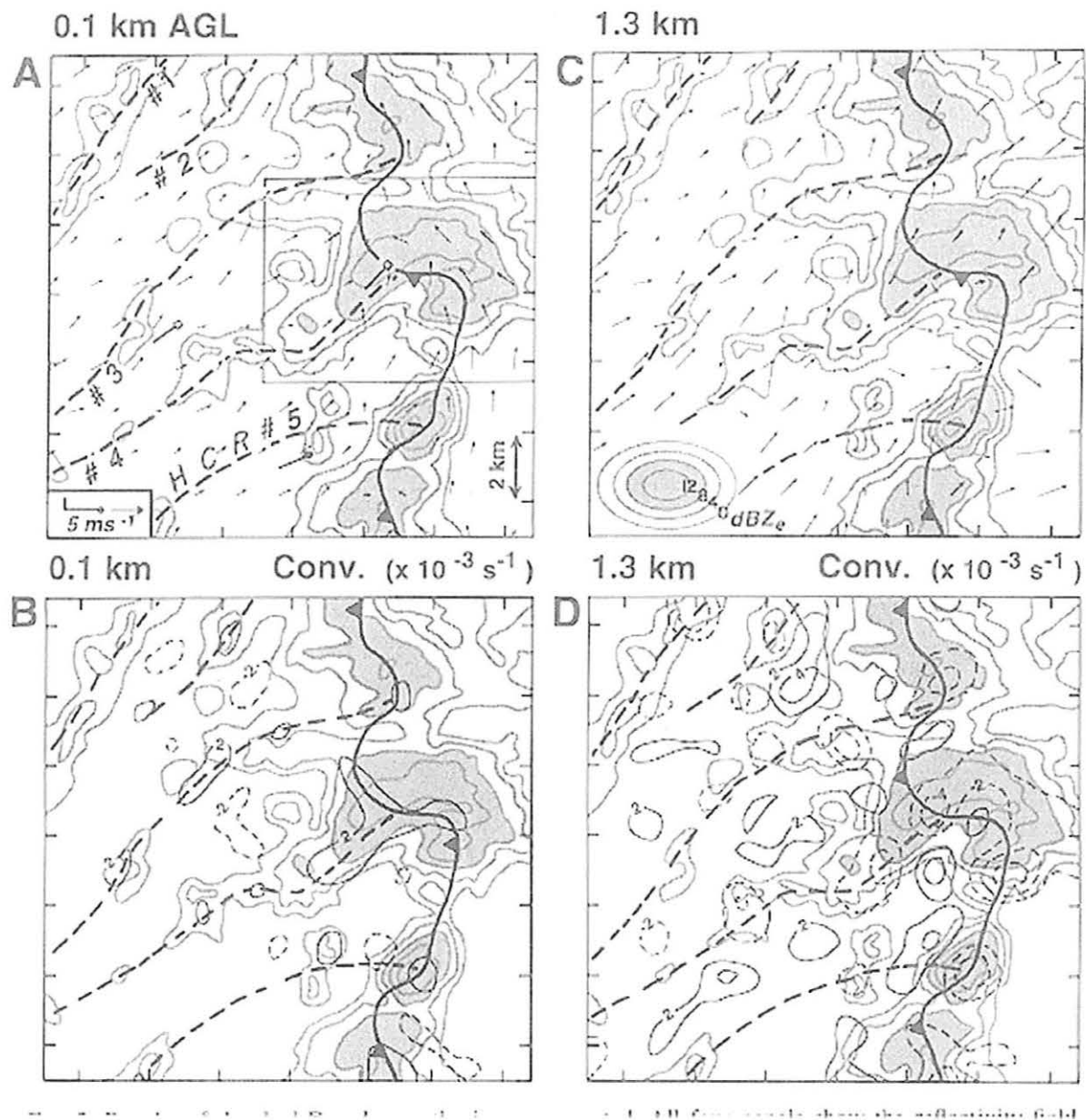


Fig. 36. Example of horizontal convective rolls intersecting a sea breeze front (after Atkins et al. 1995).

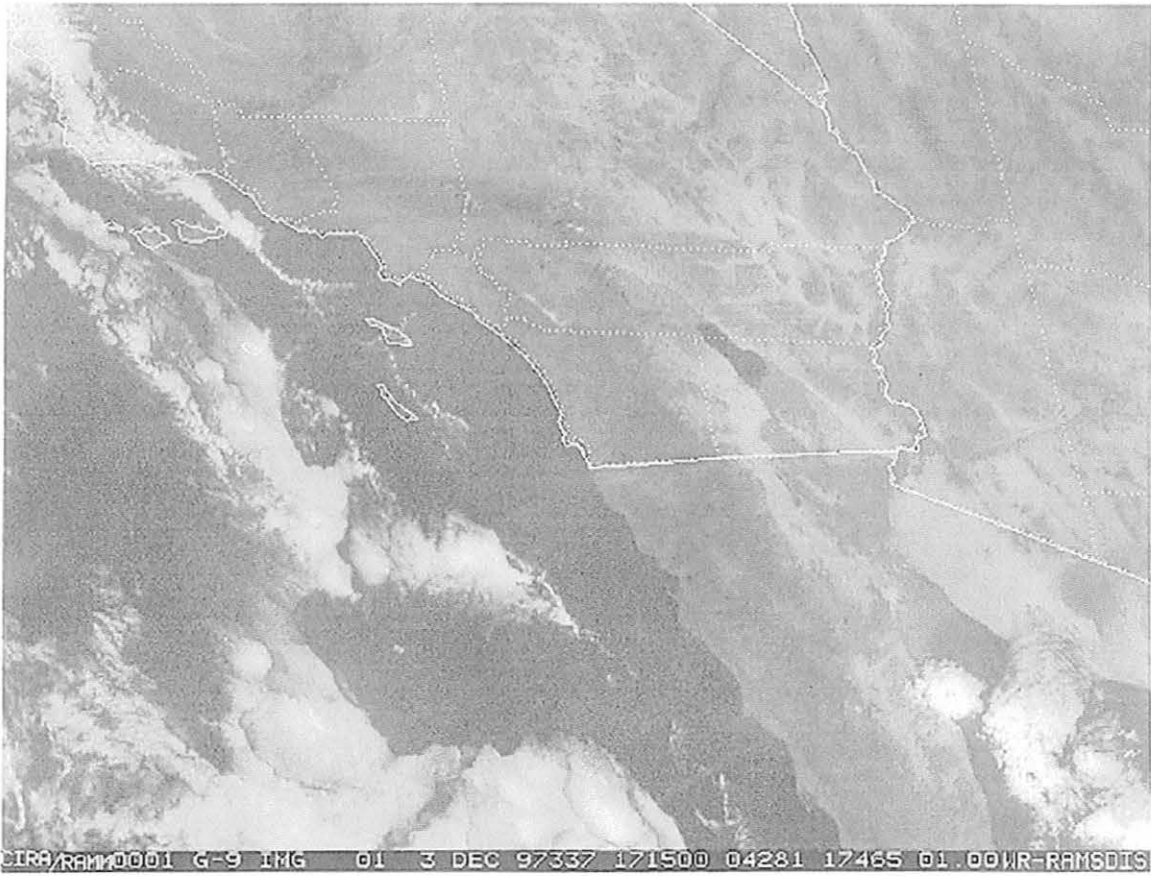


Fig. 37. 1715 UTC 3 December 1997 1 km visible satellite imagery

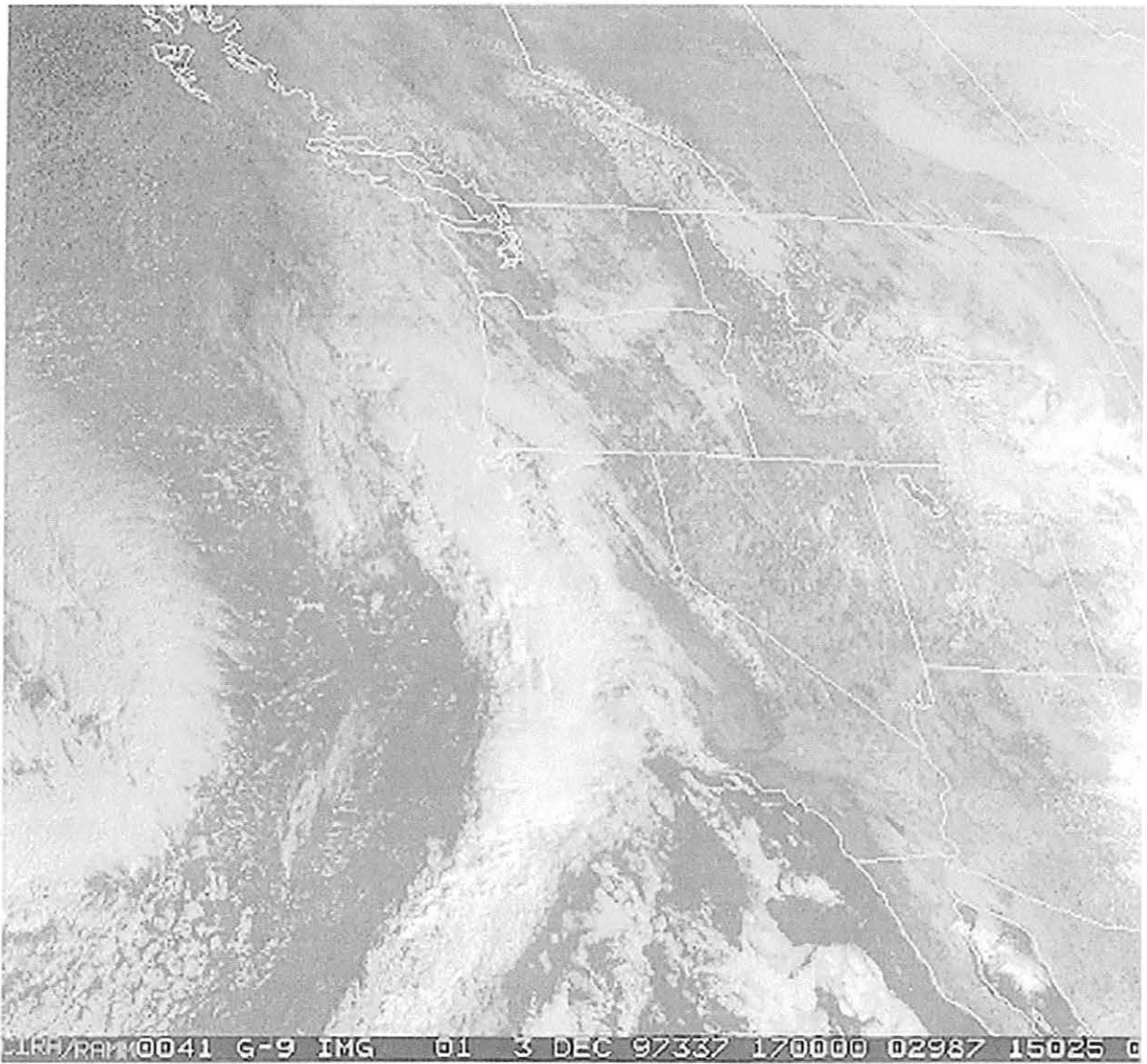


Fig. 38. 1700 UTC 3 December 1997 4 km visible satellite imagery

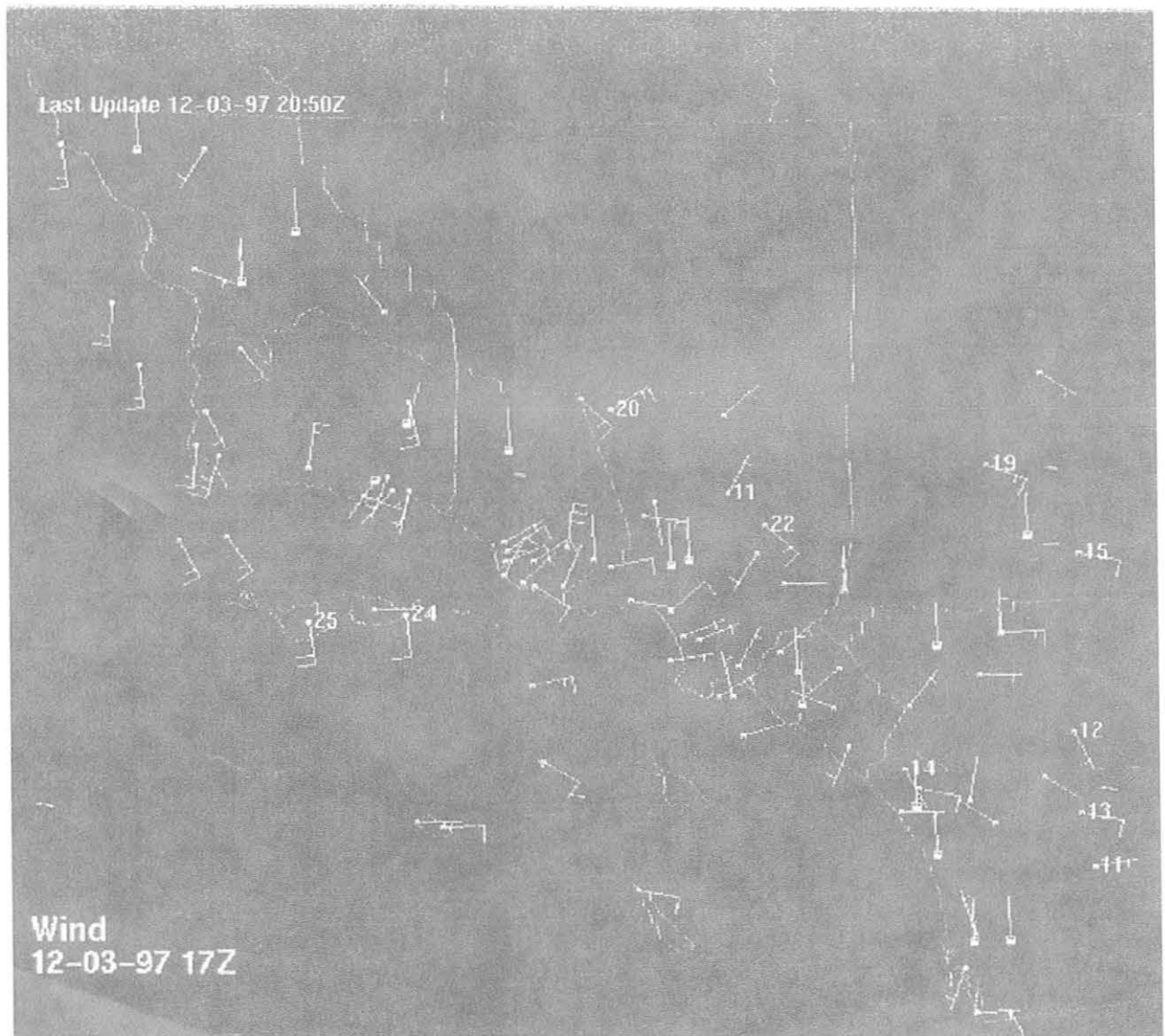


Fig. 39. 1700 UTC 3 December 1997 ALERT surface winds. Wind gusts are indicated adjacent to the station plots where gusts occurred.

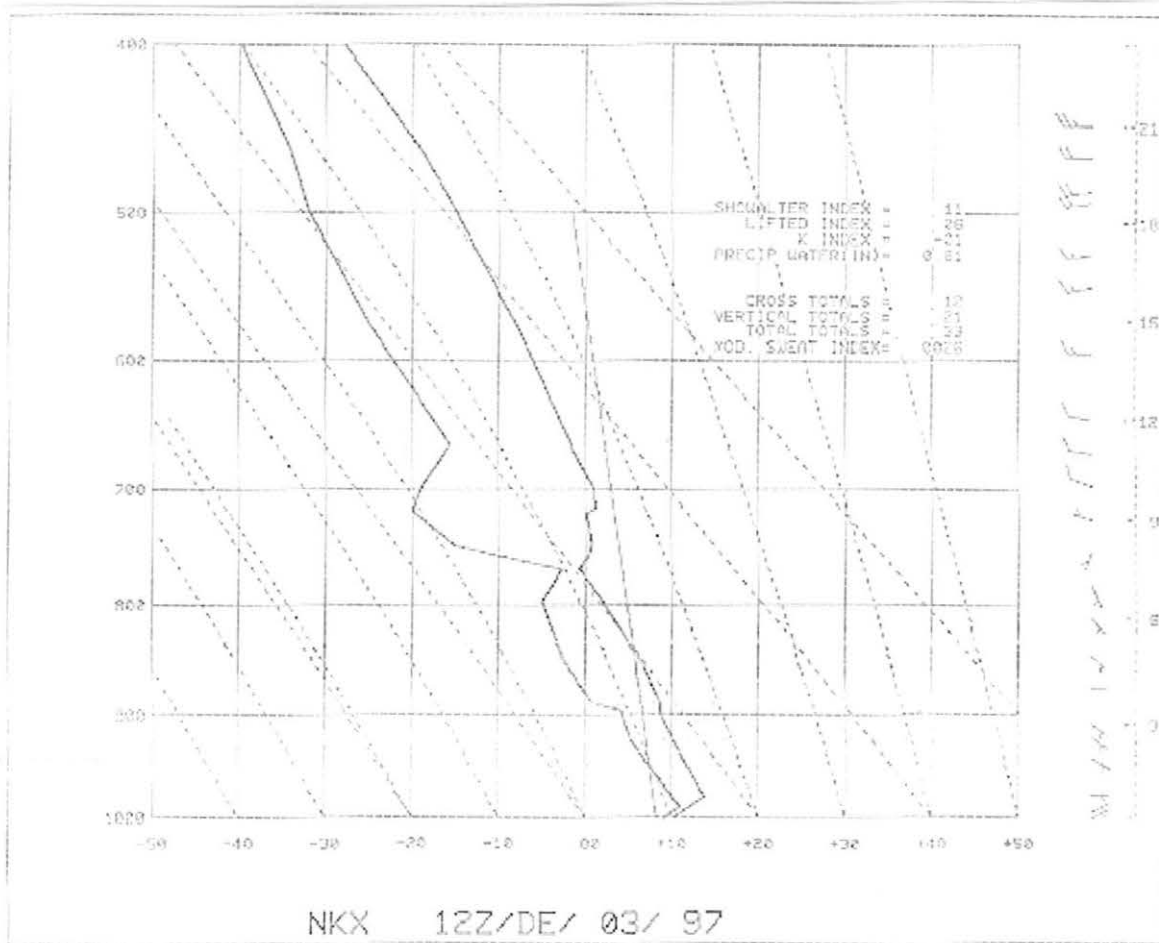


Fig. 40. 1200 UTC 3 December 1997 NKX raob

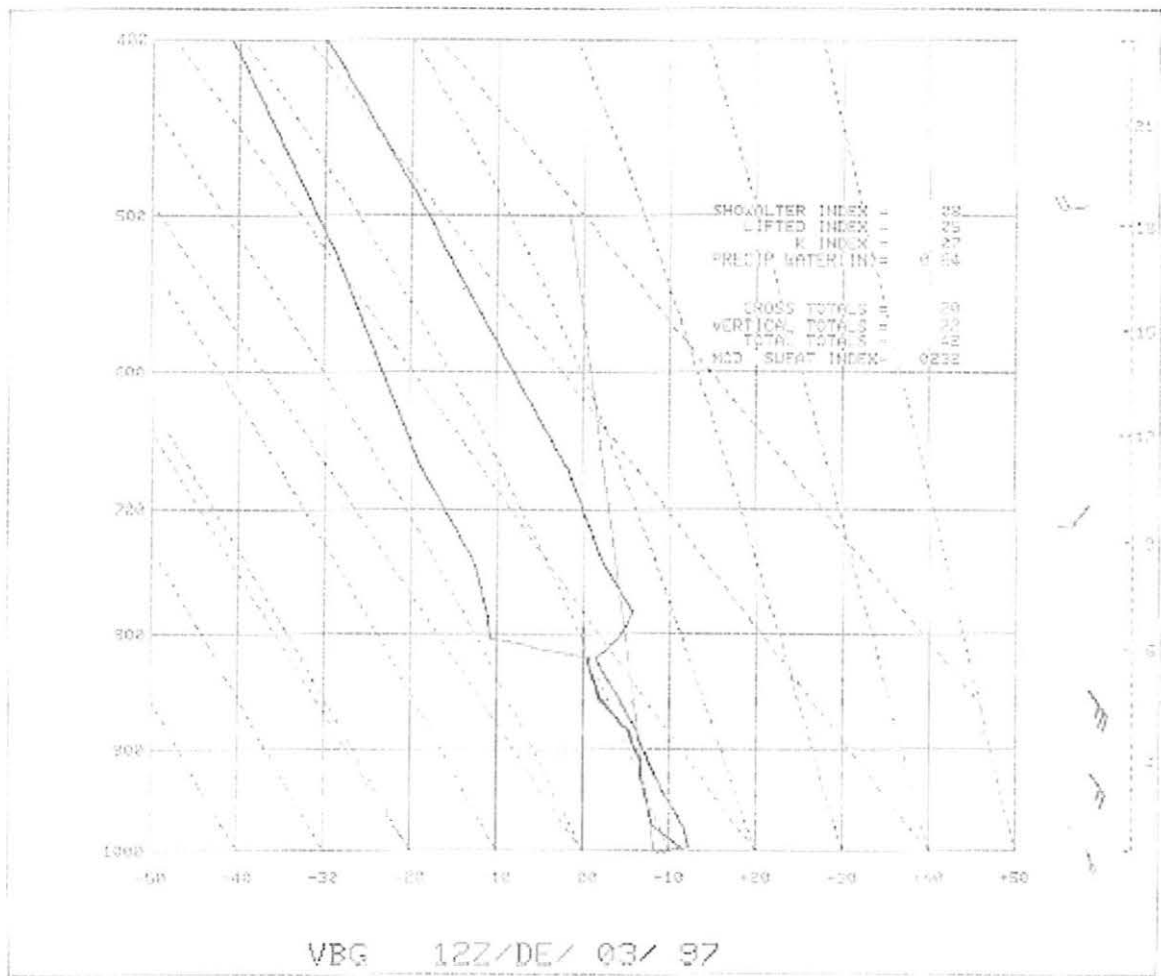


Fig. 41. 1200 UTC 3 December 1997 VBG raob

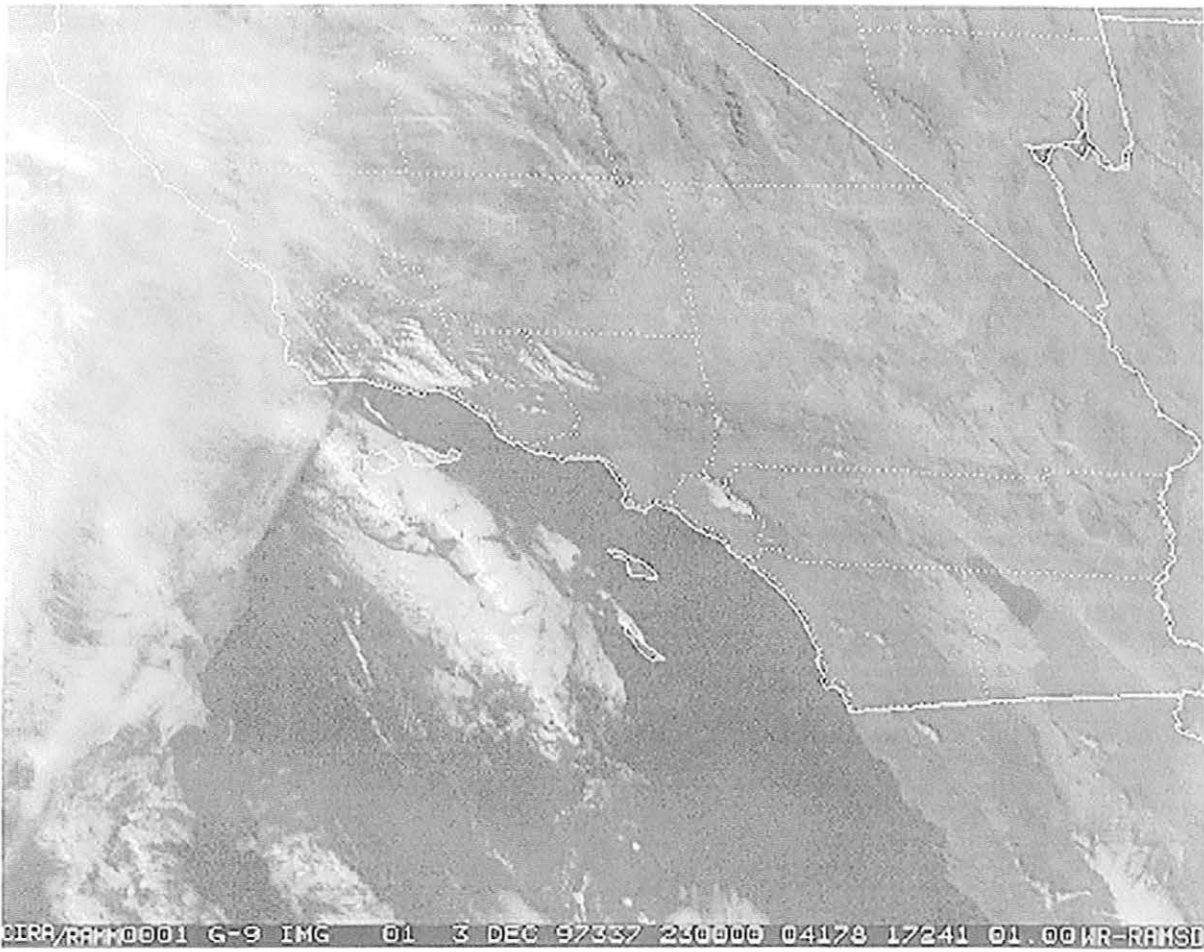


Fig. 42. 2300 UTC 3 December 1997 1 km visible satellite imagery.

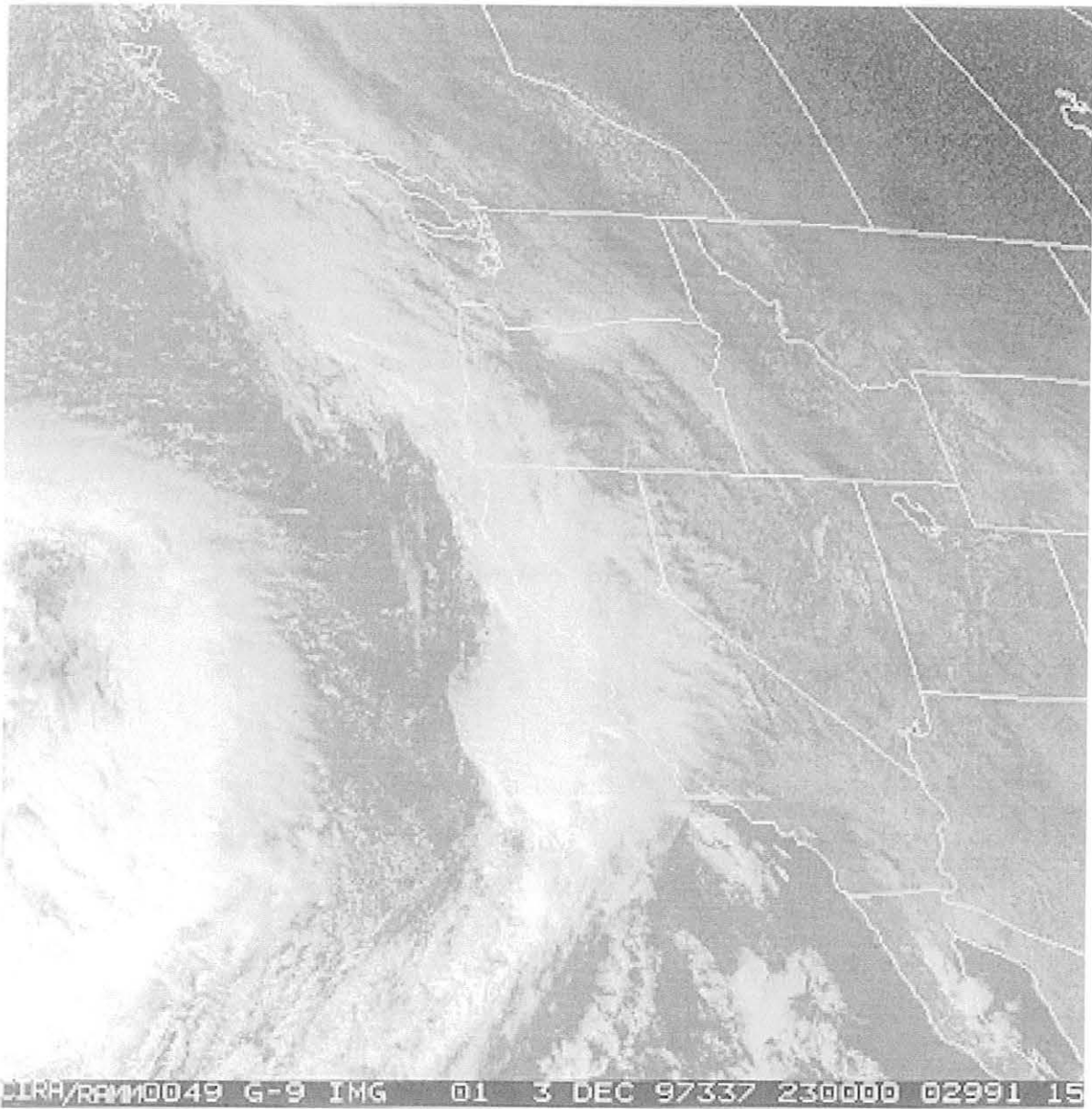


Fig. 43. 2300 UTC 3 December 1997 4 km visible satellite imagery

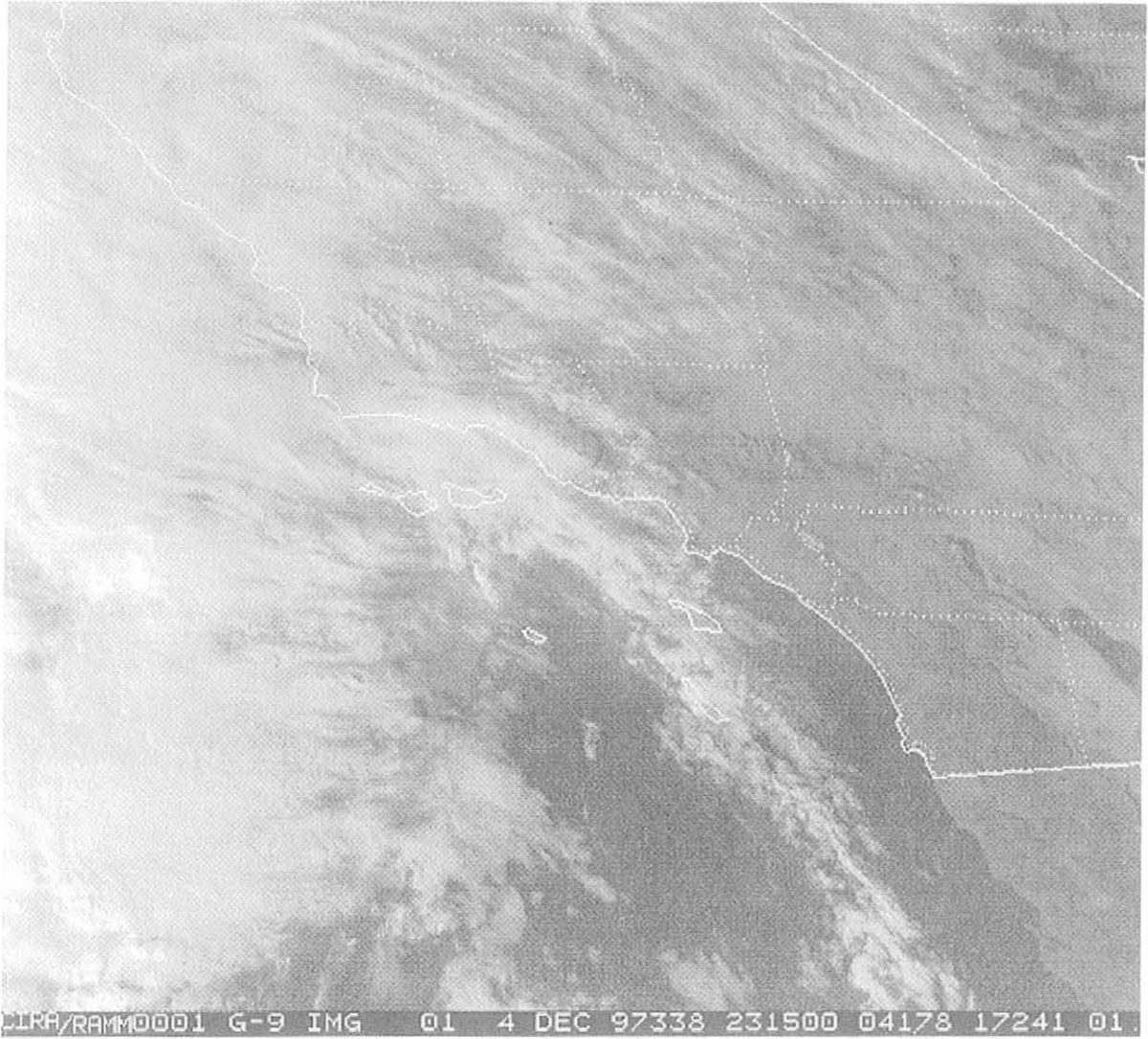


Fig. 44. 2315 UTC 4 December 1997 1 km visible satellite imagery

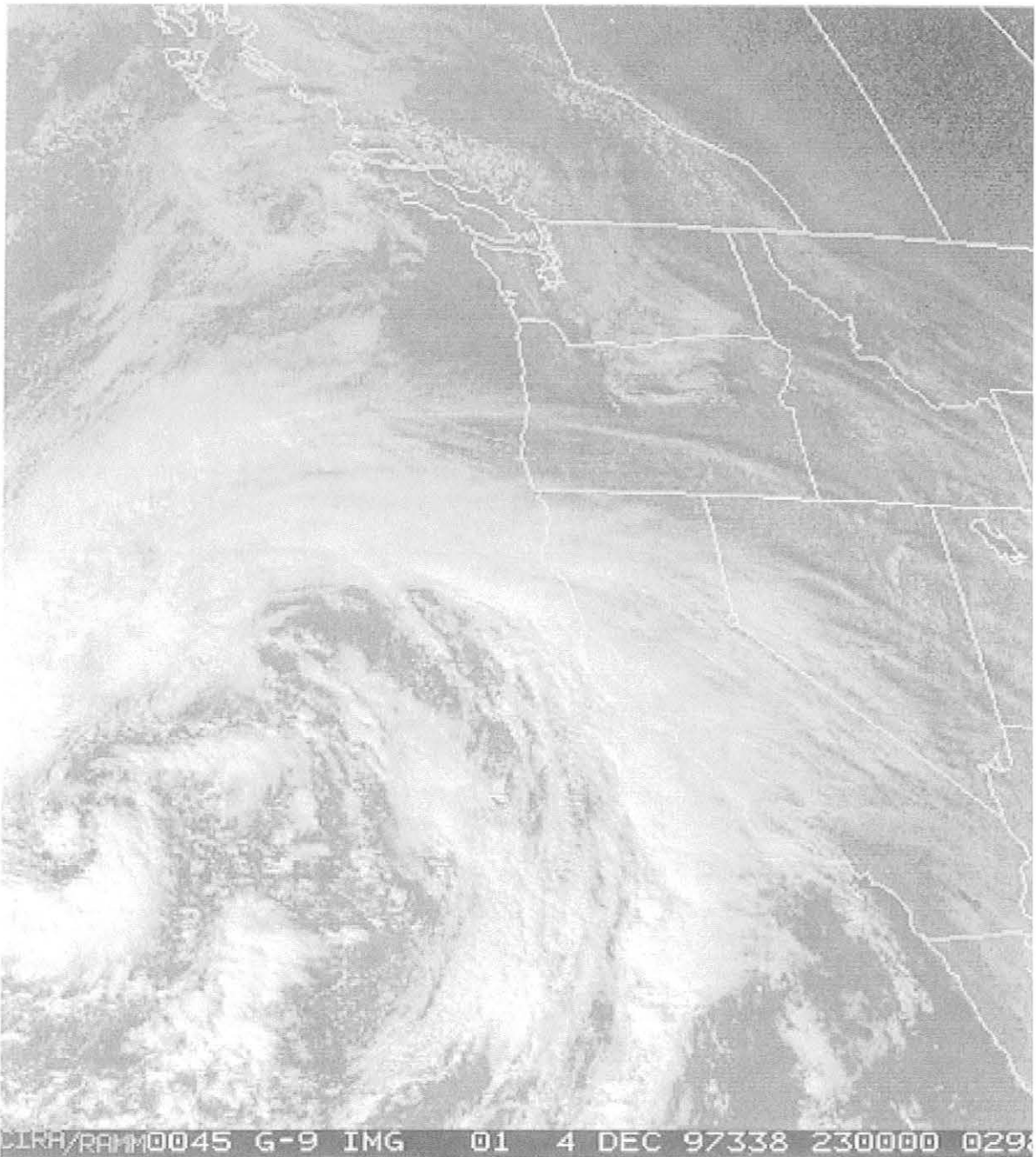


Fig. 45. 2300 UTC 4 December 1997 4 km visible satellite imagery

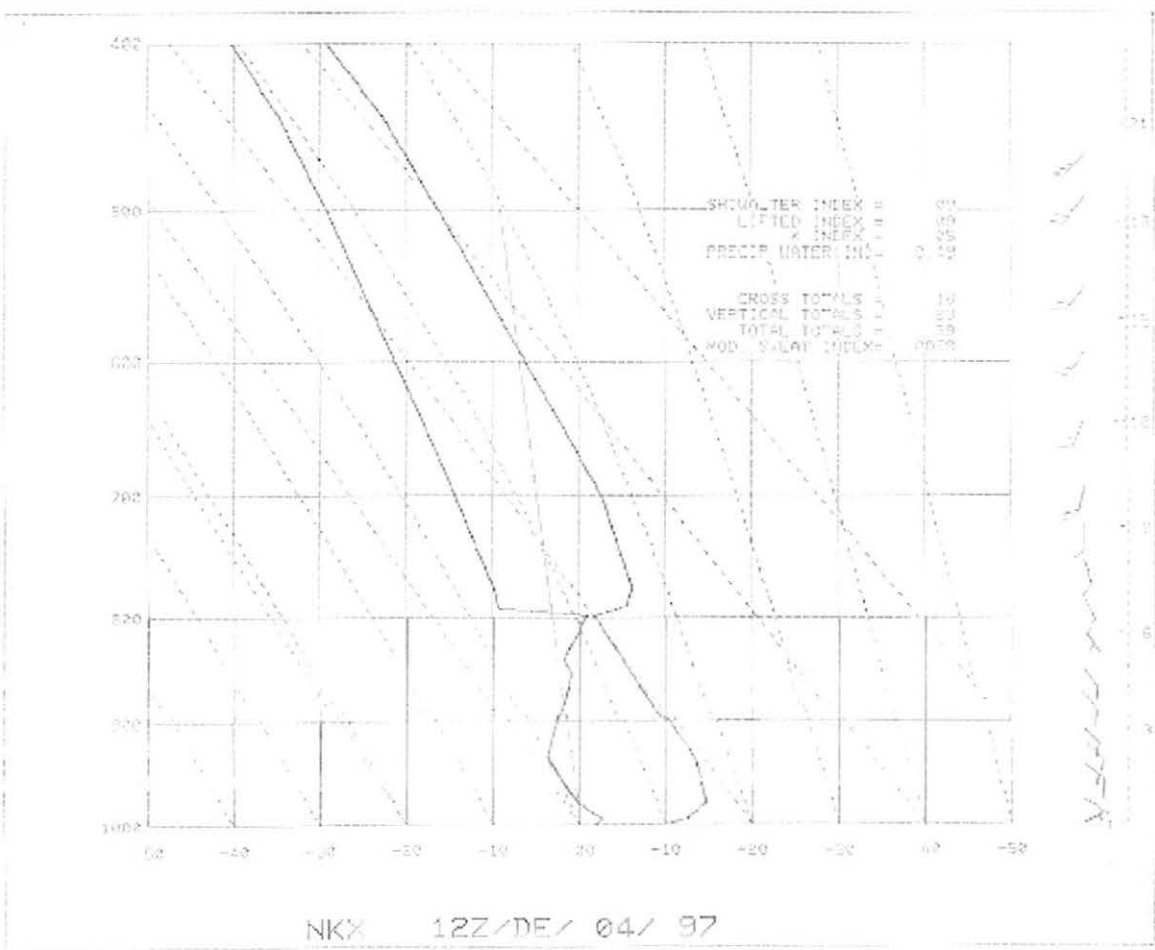


Fig. 46. 1200 UTC 4 December 1997 NKX raob



Fig. 47. 1200 UTC 4 December 1997 VBG raob